Science Translational Medicine 2020 ;Volum 12:eabb0580.(565) s. 1-13 (DOI: 10.1126/scitranslmed.abb0580)

Engineering of human albumin for enhanced half-life and transmucosal delivery of protein-based biologics

Malin Bern[1,2,], Mattia Ferrarese[4#], Jeannette Nilsen[1,2#], Kine M. K. Sand[1,2,3#], Torleif T. Gjølberg[1,2,5$], Heidrun E. Lode[1,2,5$], Robert J. Davidson[6], Rodney M. Camire[6,7], Espen S. Bækkevold[8], Stian Foss[1,2,3], Algirdas Grevys[1,2,3], Bjørn Dalhus[9], John Wilson[10], Lene S. Høydahl[11], Gregory J. Christianson[10], Derry C. Roopenian[10], Tilman Schlothauer[12], Terje E. Michaelsen[13,14], Morten C. Moe[5], Silvia Lombardi[4], Mirko Pinotti[4], Inger Sandlie[1,3], Alessio Branchini[4*] and Jan Terje Andersen[1,2*]

[1]Centre for Immune Regulation (CIR) and Department of Immunology, University of Oslo and Oslo University Hospital Rikshospitalet, Oslo, Norway.

[2]Institute of Clinical Medicine and Department of Pharmacology, University of Oslo and Oslo University Hospital, Oslo, Norway.

[3]CIR and Department of Biosciences, University of Oslo, Norway.

[4]Department of Life Sciences and Biotechnology, University of Ferrara, Ferrara, Italy

[5]Department of Ophthalmology, University of Oslo and Oslo University Hospital Rikshospitalet, Oslo, Norway.

[6]The Children's Hospital of Philadelphia, The Raymond G. Perelman Center for Cellular and Molecular Therapeutics, Philadelphia, Pennsylvania, USA.

[7]Department of Pediatrics, Division of Hematology, University of Pennsylvania, Philadelphia, Pennsylvania, USA.

[8]CIR and Department of Pathology, Oslo University Hospital Rikshospitalet and University of Oslo, Oslo, Norway.

[9]Department of Medical Biochemistry, Oslo University Hospital Rikshospitalet and University of Oslo, Oslo, Norway.

[10]The Jackson Laboratory, Bar Harbor, Maine 04609, USA.

[11] KG Jebsen Coeliac Disease Research Centre, University of Oslo, Norway.

[12]Biochemical and Analytical Research, Large Molecule Research, Roche Pharma Research and Early Development (pRED), Roche Innovation Center, Munich, Germany.

[13]Department of Infectious Disease Immunology, Norwegian Institute of Public Health, Oslo, Norway.

[14]Department of Chemical Pharmacy, School of Pharmacy, University of Oslo, Oslo, Norway.

#Contributed equally

$Contributed equally

*Corresponding authors

Jan Terje Andersen, Department of Immunology and Department of Pharmacology, Oslo University Hospital Rikshospitalet and University of Oslo, Norway, PO Box 4950, 0424 Oslo, Norway. E-mail: j.t.andersen@medisin.uio.no. Alessio Branchini, Department of Life Sciences and Biotechnology, University of Ferrara, Italy. E-mail: brnlss@unife.it.

Keywords: FcRn, albumin, IgG, engineering, transcytosis, mucosal delivery

One sentence abstract: Designed albumin enhances half-life and mucosal delivery of protein-based biologics

Abstract

Needle-free uptake across mucosal barriers is a preferred route of delivery of biologics, but the efficiency of transmucosal transport is very poor if unassisted. To make administration and therapy efficient, cost-effective and convenient, there is a need for strategies to enhance transcellular delivery but also plasma half-life. Here we report that human albumin is transcytosed efficiently across polarized epithelial cells by a mechanism that depends on FcRn. Importantly, FcRn also transports IgG, but less efficiently. This finding encouraged design of a human albumin variant (QMP) with improved receptor binding that translated into enhanced transcellular transport in human FcRn transgenic mice. In addition, QMP showed extended plasma half-life. When QMP was fused to recombinant activated coagulation factor VII (rFVIIa), the half-life of the fusion molecule increased almost 4-fold compared with the wild-type human albumin fusion, without compromising the therapeutic properties of the coagulation factor. Our findings point to QMP as an ideal carrier of biologics for enhanced plasma half-life and delivery across mucosal barriers.

Introduction

Mucosal membranes form barriers between the external environment and the interior of the body. These surfaces are composed of polarized epithelial cells that prohibit passage of pathogens while permitting selective flux of water, ions and solutes (*1*). Needle-free mucosal delivery of biologics is clearly advantageous as it is convenient, safe and cost effective. As the transport capacity across the barriers is poor, there is a need for strategies to improve uptake and transcellular delivery (*2*). However, proteins may cross the selective barriers by receptor-mediated transcytosis. The neonatal Fc receptor (FcRn) is one such membrane-bound receptor, which is required for transcytosis of maternal immunoglobulin G (IgG) to the offspring, and as such provides the fetus and newborn with humoral immune protection before its immune system is fully developed. In rats, mother's milk-derived IgGs are transcytosed across the intestinal epithelium of suckling neonatal rats, while in humans, IgG is shuttled across both placental syncytiotrophoblasts and fetal endothelium for delivery to the fetus (*3-5*). However, human FcRn is also expressed in endothelial cells of adults, and several human tissues, including mucosal epithelial cells in lungs, intestine and vagina (*6-9*). FcRn transports monomeric IgG but also IgGs bound to cognate antigens that are shuttled across epithelial barriers (*6, 7, 9-12*). While monomeric IgG may be delivered to the systemic circulation, IgG-containing immune complexes can be delivered to the lamina propria for processing by dendritic cells followed by antigen presentation to T cells (*6, 10, 12*). Thus, luminal antigens are scavenged by IgG in an FcRn-dependent manner for recognition by the immune system. This active carrier system has opened new possibilities for delivery of bioactive proteins through epithelial barriers, and a large body of evidence demonstrates that this gateway may be utilized for delivery of IgG Fc fused therapeutics and subunit vaccines (*13-19*). In all cases, FcRn has been shown to be required for delivery and therapeutic effect in pre-clinical human FcRn transgenic mice and non-human primates.

FcRn-mediated transcytosis relies on fluid-phase pinocytosis of IgG on one side of the polarized cell layer followed by pH dependent binding to FcRn, which is predominantly found within acidified endosomal compartments (*20-23*). The low pH in these endosomes triggers binding and transcytosis of the complexes to the opposite side of the cell where IgG is released upon exposure to physiological pH (*24, 25*). This strictly pH dependent process rescues IgG from intracellular degradation and secures delivery of intact antibody across the cells. The same principle of pH dependent binding and release underlies FcRn-mediated recycling that takes place in several types of cells including the vascular endothelia (*26*), which is responsible for the 3-week long half-life of IgG in humans (*27*).

The long half-life is a feature which IgG shares with only one other protein, namely albumin (*28*). Now it is established that FcRn binds not only IgG but also albumin in a similar pH dependent manner (*29-33*), and simultaneously and in a non-cooperative manner *in vitro* (*29, 30, 34*). Hence, FcRn has evolved to salvage the two most abundant proteins found in blood, which are completely unrelated both regarding structure and function. While IgG is the dominant class of antibody in the blood and fights infections, albumin acts as a multi-transporter of small insoluble substances such as fatty acids, metals and hormones as well as a wide range of drugs (*35, 36*). The finding that FcRn acts as a receptor for albumin has inspired research into how it regulates albumin transport and biodistribution, and in particular, whether or not FcRn mediates transcytosis of albumin across cellular barriers. These are highly relevant questions, as albumin is increasingly utilized as a therapeutic molecule, either as a carrier of conjugated or genetically fused drugs or as a building block for biodegradable nanoparticles (*37*). If albumin is transported across mucosal epithelia in a receptor-specific manner, it may allow for delivery of albumin-based biologics.

Here, we show that human albumin is indeed shuttled across epithelial barriers, and surprisingly, more efficiently so than IgG. We demonstrate that the efficient transcytosis of

both human albumin and fusions depends on binding to FcRn and the pH gradient within the endosomal pathway. Importantly, an albumin variant (QMP) engineered for improved pH dependent FcRn binding showed increased transport capacity. The engineered albumin was delivered to the circulation upon intranasal (i.n.) delivery more efficiently than wild-type (WT) albumin *in vivo* in human FcRn transgenic mice. In addition, QMP showed greatly enhanced plasma half-life. When QMP was fused to recombinant activated coagulation factor VII (rFVIIa), the half-life of the fusion molecule increased almost 4-fold compared with the WT human albumin fusion. Thus, targeting to FcRn using QMP should be an attractive strategy for convenient delivery and enhanced plasma half-life of protein-based biologics.

Results

FcRn enhances transport of albumin across polarized human epithelial cells

Human FcRn has been found in epithelial cells lining mucosal surfaces, including the intestine and lung (*6-9, 15*). In line with this, staining of frozen tissue sections from the human intestine, vagina and rectum using an Alexa 647 conjugated Fab fragment of ADM31, a monoclonal antibody specific for the albumin binding site on human FcRn, confirmed its presence (Fig. S1e-g).

To address whether or not albumin is transcytosed across polarized human epithelial cells, we took advantage of the colon-derived epithelial cell line T84, which polarizes within a few days and expresses FcRn (*11*). Expression was confirmed by staining with monoclonal anti-FcRn antibodies with specificity for the albumin binding site (ADM31) or IgG binding site (DVN24) (Fig. S1a-c). T84 cells are in a "non-inflammatory state", as they express neither invariant chain nor classical Fcγ receptors (*11*) (Fig. S2). They have previously been utilized in studies of bi-directional transcytosis of IgG variants (*11*), using a transwell assay (Fig. S3). In addition to WT albumin, we utilized an engineered albumin variant with two point mutations within the C-terminal domain III (DIII) (K500A/H510Q (KAHQ)) (Fig. 1a), which should abolish binding to FcRn. Both molecules were produced and secreted from Human Embryonic Kidney 293E (HEK293E) cells after transient transfection followed by purification. The albumin variants migrated according to their molecular weights as revealed by SDS-PAGE analysis (Fig. 1b), and as expected, the WT but not the double mutant bound human FcRn at acidic pH (Fig. 1c). Next, the amounts of albumin transported across the epithelial cells were quantified using an anti-albumin two-way ELISA. Bidirectional transport was measured by adding albumin variants to the apical or to the basolateral chamber (time 0) and collecting samples from the opposite chamber after 4 hours. The results showed that albumin was transported in both directions, however, the transport was 3-fold more

efficient from the apical to the basolateral side than vice versa (Fig. 1d). 2-fold more WT albumin than KAHQ was transported, which demonstrated FcRn-dependence (Fig. 1e). Furthermore, transport of albumin was measured in the presence of ADM31, which reduced transcytosis to the same extend as KAHQ, while the addition of DVN24 or an isotype control did not influence transport (Fig. 1f).

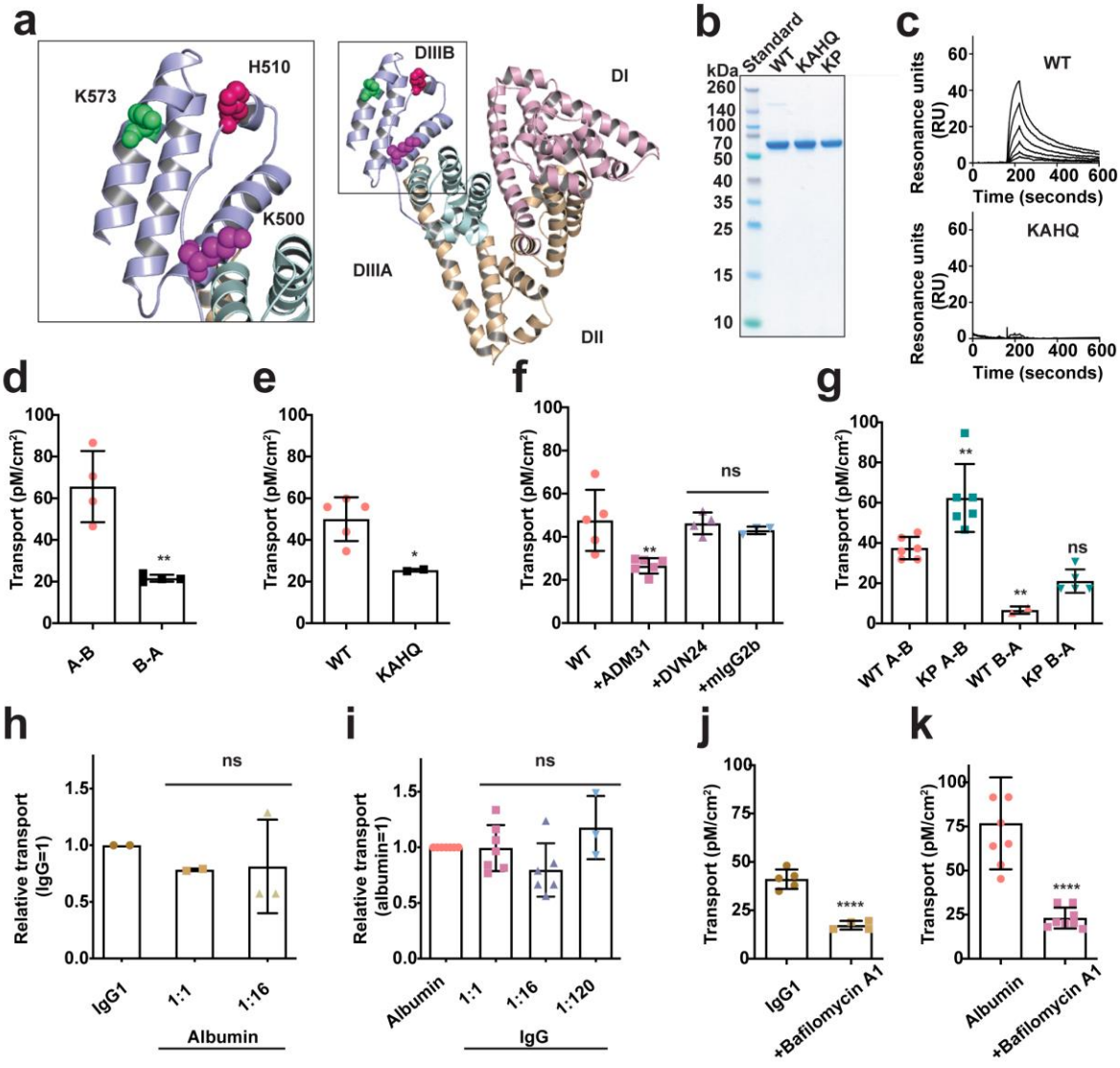

Figure 1 | FcRn enhances transport of albumin across polarized human epithelial cells. (**a**) The crystal structure of human serum albumin (PDB code 1BM0) with domain one, two

and three (DI, DII and DIII) highlighted in pink, orange and cyan/blue, respectively. A close-up of DIII is shown and is split into sub-domains DIIIa (cyan) and DIIIb (blue). Coloured spheres in DIII show amino acids targeted by mutagenesis; H510 (pink) and K500 (magneta) and K573 (green). (**b**) Non-reducing SDS-PAGE gel showing migration of the albumin variants. (**c**) SPR sensorgrams showing binding of titrated amounts of monomeric His-tagged human FcRn injected over immobilized albumin variants at pH 5.5. (**d**) ELISA quantification of the amounts of albumin transported from the apical to basolateral side (A-B) or the basolateral to apical side (B-A) of polarized T84 monolayers 4 hours post sample addition. (**e**) A-B transport of WT and KAHQ, (**f**) A-B transport of WT alone and in the presence of anti-human FcRn antibodies or mouse IgG2b (mIgG2b) and (**g**) A-B and B-A transport of WT albumin and the KP mutant. (**h**) ELISA quantification of the amounts of apical to basolateral (A-B) transport of human IgG1 (hIgG1) across polarized T84 monolayers after 4 hours, in the presence of albumin in molar ratio 1:1 and 1:16. (**i**) ELISA quantification of the amounts of A-B transport of albumin across polarized T84 monolayers after 4 hours, in the presence of increased amounts of IgG1 in molar ratio 1:1, 1:16 and 1:120. (**j-k**) ELISA quantification of the amounts of A-B transport of hIgG1 (**j**) and albumin (**k**) across polarized T84 monolayers after 4 hours with 0.1 µM bafilomycin A1. Error bars indicate S.D. of up to six individual monolayers from one representative experiment out of three. *p <0.05, **p < 0.01, ***p < 0.001, ****p < 0.0001, ns: not significant, by unpaired T-test (**d-e,** and **j-k**) or one-way ANOVA test (Dunnett`s) (**f-i**).

We previously reported on an human albumin variant, with a single point mutation in the last C-terminal α-helix of DIII (K573P (KP)) (Fig. 1a), which improves binding to human FcRn at pH 5.5 by 14-fold and extends the half-life in cynomolgus monkeys from 5.4 to 8.8 days (*38*). We tested whether this engineered variant was more efficiently transcytosed than WT

albumin, and indeed, the KP substitution resulted in almost 2-fold more efficient apical to basolateral transport, as well as enhanced basolateral to apical transport (Fig. 1g).

IgG does not affect albumin transcytosis

In vitro interaction studies have shown that albumin and IgG bind FcRn in a non-cooperative manner to non-overlapping binding sites (*29-31*). However, no cellular studies exist on whether, and if so, how the two ligands are transcytosed as a ternary complex. To investigate this, we measured if apical to basolateral transport of albumin was affected by the presence of titrated amounts of WT human IgG1, and vice versa, if the presence of albumin affected IgG1 transport. The results showed that the presence of excess molar amounts of neither ligand affected transport of the other. Specifically, when 120-fold more IgG than albumin was present in the medium, similar amounts of albumin were transported (Fig. 1h-i). Furthermore, treatment of cells with Bafilomycin A1, a specific inhibitor of the vacuolar H+ ATPase that disrupts the endosomal pH-gradient (*39*), reduced transcellular transport of both IgG and albumin (Fig. 1j-k).

Mucosal delivery and uptake into blood

We have previously demonstrated that conventional rodents have limited utility as models for studies of human albumin biology due to large cross-species FcRn binding differences (*38, 40*). Thus, to address whether human albumin is taken up at a mucosal site to enter the blood *in vivo*, we took advantage of a human FcRn transgenic mouse model that lacks expression of both mouse FcRn and mouse albumin (*41, 42*). We chose to target the airways by i.n. delivery followed by inhalation. Importantly, human FcRn is expressed in lung tissues of these mice (*43*).

Administration of a droplet of Evans Blue solution to each nostril followed by dissection 20 minutes later showed pulmonary staining, which confirms that this delivery route targets the lungs (Fig. S4). We next administrated WT and KAHQ albumin i.n. and quantified their presence in blood over time (Fig. 2a). Up to 4-fold more WT albumin was detected during the first 24 hours compared with the non-binder KAHQ (Fig. 2b-c). Strikingly, 7-fold more of the WT was detected on day 4 post administration, which was the time point with the highest level detected, corresponding to roughly 25% of the amount given (Fig. 2c).

To further confirm the involvement of FcRn in pulmonary uptake of albumin, we repeated the experiment in mice that lack expression of the receptor. As expected, WT albumin was detected at lower and comparable levels to that of the non-binder KAHQ (Fig. S5a).

Next, equimolar amounts of WT albumin and human IgG1 (anti-NIP) were given i.n. to the human FcRn transgenic mice followed by sampling of blood at 4, 8 and 24 hours as well as after 6 days. Markedly, as much as 4-fold more albumin than IgG was detected in blood after 4 hours, which increased to more than 8-fold from 8 hours to 6 days (Fig 2d-e). Interestingly, even in the absence of FcRn expression, 2-fold more albumin than IgG1 was detected (Fig. S5b).

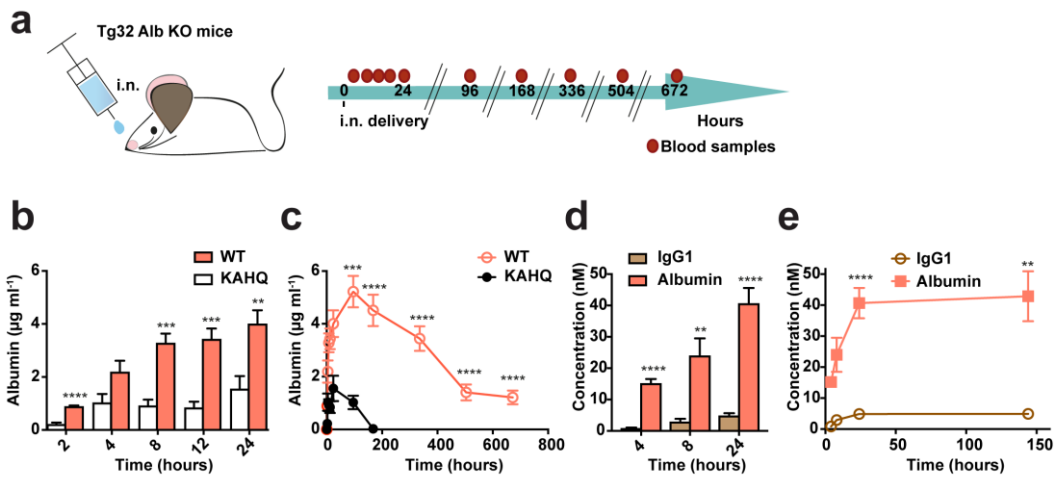

Figure 2 | Mucosal delivery of albumin and uptake into blood *in vivo.*

(**a**) A schematic drawing of i.n. delivery of albumin to human FcRn transgenic mice without albumin expression and flow chart of the i.n. delivery protocol followed by blood sampling. Levels (μg ml^{-1}) of albumin in blood at the first 24-hour time points (**b**) and all time points (**c**). Levels (nM) of albumin and IgG in blood at the first 24-hour time points (**d**) and all time points (**e**). Albumin variants and IgG were given i.n. at a single dose with 5 mice per group. *p <0.05, **p < 0.01, ***p < 0.001, ****p < 0.0001, ns: not significant, by unpaired T-test. Data are presented as mean ± s.e.m. of five mice from one experiment.

Efficient transcytosis of albumin fusion proteins

As the data pointed to FcRn as a vehicle for delivery of albumin-fused drugs, we tested whether albumin with a C-terminally fused glutathione-S transferase (GST) (26 kDa) could be delivered across T84 cells (Fig. 3a). GST was fused to both WT albumin and KAHQ, and purified proteins migrated with expected molecular weights in SDS-PAGE (Fig. 3b). Using ELISA, pH dependent binding to human FcRn was confirmed for the WT-fusion, while the KAHQ-fusion did not bind (Fig. 3c). Next, the two GST-fusions were added to the apical side of polarized T84 cells in the Transwell system, and by quantifying the amounts released on the basolateral side, we demonstrated that the WT-fusion was shuttled across the cell layer 4-fold more efficiently than KAHQ (Fig. 3d).

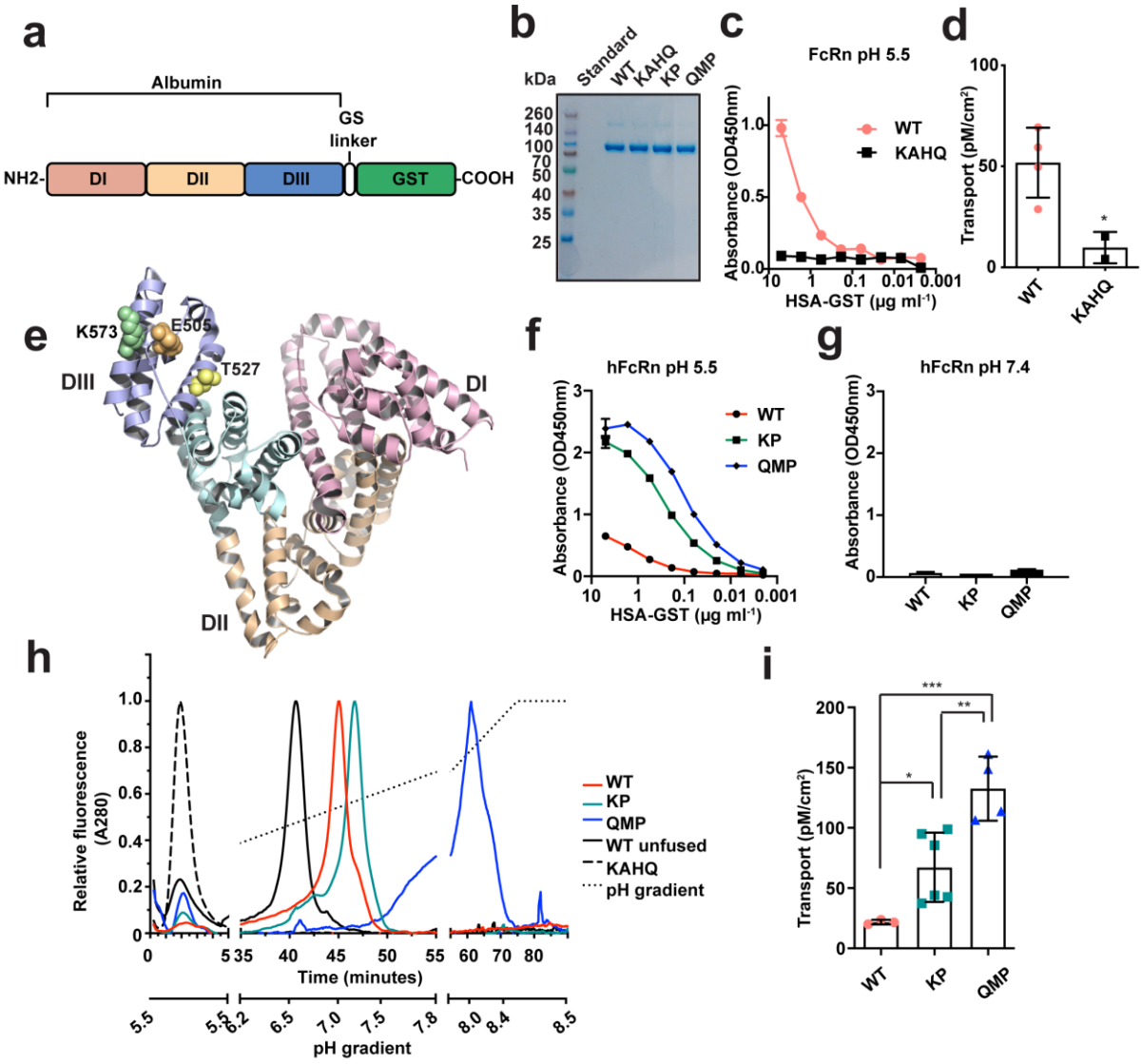

279

280 **Figure 3 | Transport of engineered albumin fusion proteins.** (**a**) Schematic illustration of
281 the fusion protein showing the three human albumin domains (DI, DII and DIII) followed by
282 a glycine-serine (GS)-linker and the GST-tag. (**b**) Non-reducing SDS-PAGE gel showing
283 migration of monomeric fractions of albumin-GST fusion variants (93 kDa). (**c**) Binding of
284 His-tagged human FcRn (10 µg ml^{-1}) to titrated amounts (5-0,002 µg ml^{-1}) of albumin-GST
285 variants at pH 5.5. Data are presented as mean ± S.D. (**d**) ELISA quantification of the
286 amounts of A-B transport of GST-WT and GST-KAHQ albumin across polarized T84
287 monolayers after 4 hours. (**e**) Crystal structure of human serum albumin with DI, DII and
288 DIII highlighted in pink orange and cyan, respectively. Coloured spheres in DIII show amino

acid positions that have been mutated; K573 (green), E505 (orange) and T527 (yellow). (**f-g**) Binding of His-tagged human FcRn (10 μg ml^{-1}) to titrated amounts (5-0,002 μg ml^{-1}) (**f**) or 5μg ml^{-1} (**g**) of albumin-GST variants at pH 5.5 (**f**) or pH 7.4 (**g**). (**h**) Elution profiles of albumin variants from an FcRn-coupled column after application of a pH gradient (5.5-8.8). (**i**) ELISA quantification of the amounts of A-B transport of GST-fused WT, KP and QMP across polarized T84 monolayers after 4 hours. Error bars indicate S.D. of up to six individual monolayers from one representative experiment out of three. *p <0.05, **p < 0.01, ***p < 0.001, ****p < 0.0001, ns: not significant, by unpaired T-test (**d**) or one-way ANOVA test (Dunnett`s) (**i**).

Engineered human albumin with improved FcRn binding

To investigate whether albumin could be engineered for enhanced transcytosis beyond that of KP, we used a structure-based approach, and inspected a previously published docking model of the FcRn-albumin complex (*44*). Amino acid residues within DIII that could be targeted by site-directed mutagenesis to improve binding were identified; namely E505Q (EQ) and T527M (TM) (Fig. 3e). These were combined with KP to generate a triple mutant (QMP), which was produced in similar amounts to that of the WT-GST fusion and migrated with expected molecular weight (Fig. 3b). Circular dichroism (CD) spectroscopy revealed that none of the introduced mutations had any major influence on the composition of secondary structural elements (Fig. S6 and Table S1).

Next, we measured the effect of the introduced mutations on binding to human FcRn using ELISA (Fig. 3f), which revealed that QMP resulted in considerably increased binding at acidic pH, while barely affecting binding at neutral pH (Fig. 3g). Binding kinetics were determined by surface plasmon resonance (SPR), where titrated amounts of monomeric human FcRn were injected over immobilized albumin fusions (Table 1, Fig. S7a-c). First, we

compared the WT-fusion with that of unfused albumin (Fig. 1c), which showed that fusion to the C-terminal end only had a minor negative impact. Introduction of the KP led to 14-fold improved K_D, while QMP improved the K_D more than 180-fold (Table 1). To address the influence of the mutations on dissociation from FcRn throughout a pH gradient, we determined the elution profiles of the GST-fusions by analytical human FcRn chromatography (*45*). While unfused albumin eluted with a main peak at pH 6.5, the WT fusion showed a shift and eluted at pH 7.0 (Fig. 3h). Of the mutants, KP eluted after the WT fusion (pH 7.2), while QMP eluted at pH 8.0 (Fig. 3h). As expected, the non-binder KAHQ did not bind the column (Fig. 3h). Importantly, when we benchmarked against engineered human albumin variants reported by others, VA (547) (*46*) and IG (523) (*47*), QMP was shown to have more favorable binding and transport properties (Table 1 and Fig. S7d-i)

Table 1. SPR derived kinetics for binding of albumin variants to FcRn at pH 5.5			
Albumin variant	K_a (10^4 $M^{-1}s^{-1}$)	K_d ($10^{-3}s^{-1}$)	K_D (nM)
Human FcRn			
Unfused WT	4.3±0.1	5.4±0.1	125.6
GST WT	3.2±0.1	4.7±0.2	146.8
GST IG	3.8±0.2	0.9±0.0	23.6
GST KP	2.9±0.0	0.3±0.1	10.3
GST VA	7.4±0.1	0.7±0.0	9.5
GST QMP	12.9±0.1	0.1±0.1	0.8
scFv WT	3.9±0.3	7.8±0.4	200.0
scFv QMP	7.9±0.1	0.3±0.1	3.8
rFVIIa WT	4.6±0.1	11.4±0.1	248.0
rFVIIa QMP	12.4±0.1	0.09±0.1	0.7
Mouse FcRn			
rFVIIa WT	NA	NA	NA
rFVIIa QMP	2.0±0.1	5.8±0.2	290.0
The kinetic rate constants were obtained using a simple first-order (1:1) Langmuir bimolecular interaction model. The kinetic values represent the average of triplicates. NA, not acquired due to fast kinetics.			

Engineered albumin shows enhanced transcytosis

The transcytosis properties of the GST-fused engineered variants were compared with the WT using the polarized T84 transcytosis assay. Transport in the apical to basolateral direction was measured, as this is the route relevant for mucosal delivery to blood. Quantification of

variants on the basolateral side revealed that KP was transported at least 2-fold more efficiently than WT (Fig. 3i), while QMP was transported 4-fold more efficiently (Fig. 3i).

Next, to investigate whether QMP would be delivered more efficiently across mucosal barriers *in vivo*, we again utilized the human FcRn transgenic mice that do not express mouse albumin. We compared the blood levels of unfused WT, KAHQ and QMP over time following i.n. administration. Surprisingly, both WT and QMP were detected in blood at high levels, and there were no significant difference between the two, in spite of the fact that they have very different FcRn binding kinetics (Fig. 4a-b).

Importantly, both mice and humans have high levels of liver-produced albumin (20-40 mg/ml) in blood under normal circumstances (*28*), while the experiment was done in the absence of albumin. Thus, we speculated that the result might be due to lack of competition for FcRn binding from endogenous albumin. We thus pre-loaded the mice intraperitoneally (i.p.) with WT human albumin. Initially, two doses were given (250 mg kg^{-1} or 500 mg kg^{-1}), and since both gave stable levels of albumin over time, the lower dose was used in the following experiments (Fig. 4c). The mice were pre-loaded 48 hours before i.n. administration of site-specific biotinylated WT, KAHQ and QMP (Fig. 4d and Fig. S8a). Their serum levels were quantified, and indeed, over 2-fold more QMP reached the blood at early time points compared with WT albumin (Fig. 4e). The levels of KAHQ were about the same in the absence and presence of pre-loaded competing albumin (Fig. S8a). Notably, when the same experiment was repeated in mice lacking expression of FcRn, QMP was transported to the same level as the WT and KAHQ (Fig. S5a). Next, we reinvestigated pulmonary uptake of albumin and IgG in the presence of pre-loaded competing human albumin or IgG, respectively. The data confirmed that albumin is taken up more efficiently than IgG (Fig. S8b).

Taken together, we demonstrate that more albumin than IgG is taken up over mucosal surfaces, and that the QMP mutations enhances transcellular delivery to the blood. We also reveal the importance of ligand competition for receptor binding.

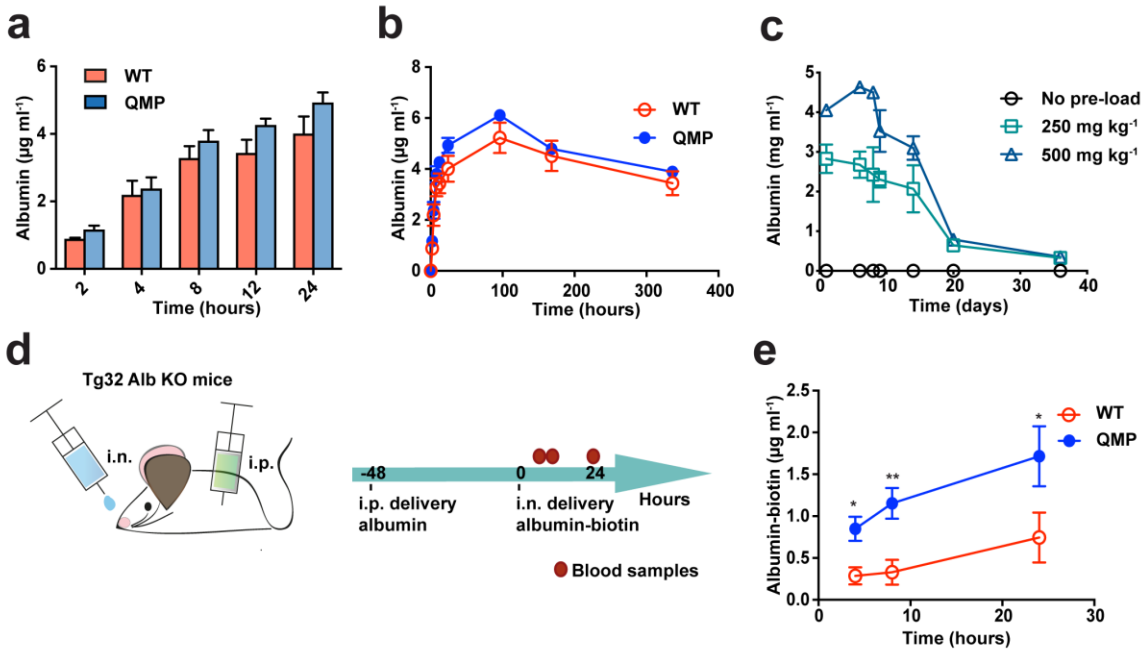

Figure 4 | FcRn-dependent mucosal uptake and half-life of engineered albumin in human FcRn Tg mice. (a-b) Levels (µg ml^{-1}) of albumin in blood derived from human FcRn transgenic mice (5 mice per group) at different time points after i.n. delivery shown in bars (**a**) and connective lines (**b**). (**c**) Levels (mg ml^{-1}) of albumin in blood of human FcRn transgenic mice (5 mice per group) at different timepoints (4, 8, 24, 96, 168 and 360 hours) after pre-load with 250 mg kg^{-1} or 500 mg kg^{-1} albumin. (**d**) An illustrative drawing of a human FcRn transgenic mouse receiving human albumin i.p. (pre-load) before i.n. delivery of albumin variants and flow chart of the i.n. delivery protocol with introduced competition (pre-load). Blood samples are taken 4, 8 and 24 hours after i.n. delivery of albumin variants. (**e**) Levels (µg ml^{-1}) of biotinylated albumin (albumin-biotin) in blood samples from human FcRn transgenic mice (5 mice per group) 4, 8 and 24 hours after i.n. delivery. *p <0.05, **p

< 0.01, ***p < 0.001, ns: not significant, by unpaired T-test. Data are presented as mean ± s.e.m. of five mice from one experiment.

Mucosal delivery of albumin fused to an antibody fragment

To test whether the FcRn-mediated mucosal pathway can be used to deliver a therapeutically relevant albumin fusion, we genetically fused an antibody-derived single-chain variable fragment (scFv), with specificity for human vascular endothelial growth factor (VEGF), to the N-terminal end of WT and QMP (Fig. S9c). The fusions bound VEGF equally well, and human FcRn in a strict pH dependent manner (Fig. 5a-c; Fig. S10a-d, Table 1). Accordingly, when the fusions were given i.n. as above to the transgenic mice that had been pre-loaded with human albumin, 4-fold more of the QMP fusion was detected in blood compared to the WT (Fig. 5d). A non-FcRn binding Fab fragment with irrelevant specificity (Fig. S9c) was not detected in blood after i.n. delivery (Fig. S10e-f). Thus, we demonstrate that the QMP albumin variant is an attractive carrier for mucosal delivery.

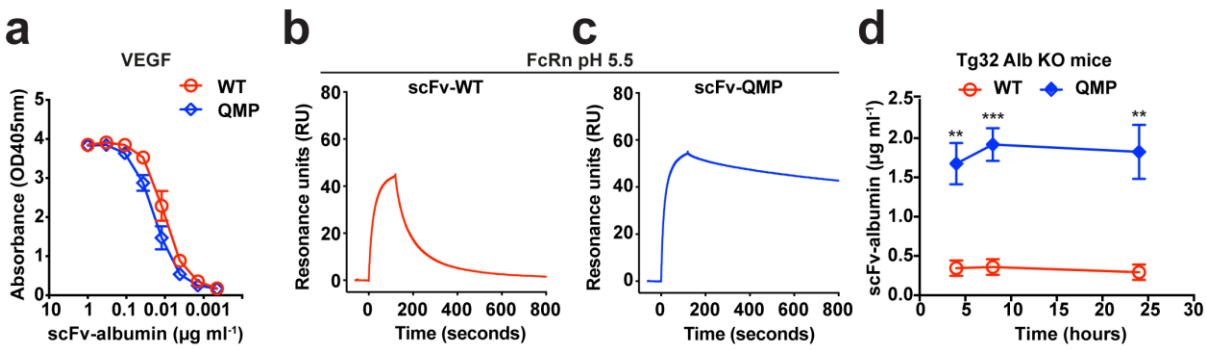

Figure 5 | Efficient mucosal delivery of an engineered antibody-albumin fusion.

(**a**) Binding of titrated amounts (1-0.00045 µg ml^{-1}) of fusion variants to VEGF coated in ELISA plates followed by detection with ALP-conjugated anti-albumin antibody. (**b-c**) SPR sensorgrams showing binding of 500 nM monomeric human FcRn injected over the

immobilized (~200 RU) scFv fused to WT albumin (**b**) or QMP (**c**) at pH 5.5. Injections were performed with a flow rate of 40 µl min^{-1} at 25°C. (**d**) Levels (µg ml^{-1}) of albumin in blood given i.n. at a single dose with 5 mice per group at 4, 8 and 24 hour time points shown in connecting lines. *p <0.05, **p < 0.01, ***p < 0.001, ns: not significant, by unpaired T-test. Data are presented as mean ± s.e.m. of five (c) or three (d) mice from one experiment.

Engineered albumin shows extended half-life

As albumin is increasingly utilized to improve the pharmacokinetics of short-lived therapeutics, we tested whether QMP would extend plasma half-life. First, we took advantage of an FcRn-dependent human endothelial recycling assay (HERA) (*32*), and found that QMP was more efficiently rescued from intracellular degradation than both WT and the KP variant (Fig. S11a). Subsequently, QMP was compared with WT and KP upon injection into human FcRn transgenic mice in the presence of competition, in which the half-life for QMP was shown to be extended by 1.2 compared with KP, with the half-life increased from 2.4 days for the WT to 4.8 days for QMP (Fig. 6a).

In the absence of competing albumin, the half-lives measured were very long, 17-20 days, for both the WT and improved variants. Specifically, the half-life of the WT was similar to that of KP while QMP showed the longest half-life (Fig. 6b). Again, this highlights the importance of the presence of competing endogenous albumin when studying pharmacokinetics of human albumin and fused biologics. Moreover, the half-life of KAHQ was short, both in the presence and absence of competing albumin (Fig. 6a-b), in line with the similarly low levels detected after i.n. delivery (Fig. S8a).

Finally, the transgenic mice were given WT albumin or QMP followed by injection of either PBS or ADM31, the monoclonal antibody that blocks the albumin binding site on FcRn (*48*). The presence of ADM31 resulted in equal and rapid clearance of both WT and QMP (Fig.

S11b-c). In accordance with this, KAHQ, WT, and QMP showed equally short half-lives after injection into mice lacking FcRn expression (Fig. 6c). Thus, engineering for improved pH dependent FcRn binding, which favours receptor engagement in the presence of competing endogenous albumin, is responsible for both enhanced transepithelial transport and extended half-life of QMP.

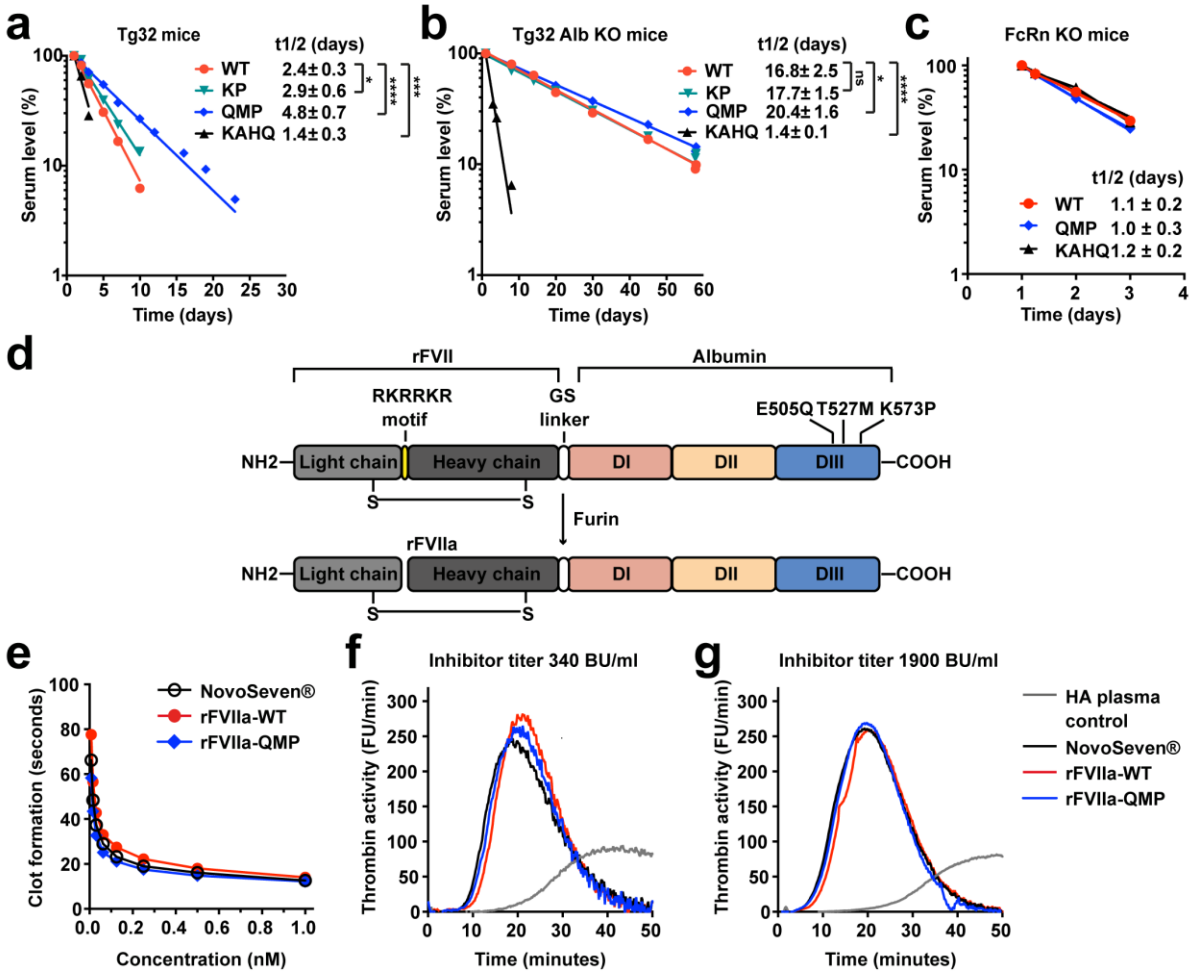

Figure 6 | rFVIIa shows retained by-passing activity when genetically fused to an engineered albumin variant. (**a-c**) Elimination curves of unfused albumin WT (red), KP (green), KAHQ (black) and QMP (blue) in human FcRn transgenic mice with (n=10, except n=5 for KAHQ) (**a**) or without (n=5) (**b**) endogenous albumin and in FcRn deficient mice (n=5) **(c)**. The serum levels are presented as percentage remaining in the circulation compared to that measured 1 day after the mice received 1-3 mg kg^{-1} via i.v. (**a, c**) or i.p. (**b**)

injection. Mean β-phase half lives ($T_{1/2}$) ± S.D. are shown in days. (**d**) Schematic illustrations showing rFVIIa genetically fused via a glycine-serine linker to the N-terminal of an engineered albumin variant. The three domains, DI, DII and DIII, of albumin and the three point mutations introduced in the C-terminal DIII (E505Q, T527M and K573P; QMP) are indicated. A RKRRKR motif was inserted into the activation site between the light and heavy chain of rFVII (upper panel), which is cleaved by furin-mediated intracellular processing when expressed, resulting in secretion of a cleaved and thus activated factor VII (rFVIIa) (lower panel). (**e**) Pro-coagulant activity in FVII-depleted plasma supplemented with titrated amounts (0.008-1 nM) of NovoSeven® (black) or rFVIIa fused to albumin WT (red) or QMP (blue). (**f-g**) By-passing activity measured through thrombin generation assays on plasma from hemophilia A patients with inhibitor titers of 340 BU/ml (**f**) or 1900 BU/ml (**g**) and supplemented with 60 nM NovoSeven® (black), rFVIIa fused to albumin WT (red) or QMP (blue) or in the absence of a recombinant factor (grey). FU, fluorescence units. *p <0.05, **p < 0.01, ***p < 0.001, ns: not significant, by unpaired T-test.

QMP prolongs the half-life of rFVIIa

The extended half-life of QMP encouraged investigation into whether the variant could be used as a fusion partner for half-life extension of biologics. To test this, we chose to genetically fuse a complex multi-domain protein, human rFVIIa, to QMP and WT albumin. While rFVIIa (NovoSeven®) is used clinically to control bleeding episodes in haemophilia patients who have developed inhibitory antibodies against standard replacement therapy (Fig. S12), its therapeutic efficacy is hampered by a very short half-life of only 2.5 hours in humans (*49*). To secure secretion of activated rFVII, we inserted a RKRRKR motif in the activation site of the coagulation factor, which triggers furin-mediated intracellular processing (Fig. 6d). Importantly, following purification (Fig. S13) the fused factor showed

the same ability as unfused rFVIIa (NovoSeven®) to restore coagulation of FVII-depleted human plasma (Fig. 6e) as well as equal ability to boost generation of thrombin in plasma from haemophilia A patients with high-titer inhibitors (Fig. 6f-g). Moreover, when tested for binding to recombinant human FcRn, both fusions bound pH dependently, but rFVIIa-QMP bound much more strongly at acidic pH (Fig. 7a-c, Fig. S14a-b, Table 1).

Furthermore, while we have previously shown that human albumin binds poorly to mouse FcRn, the engineered variant bound with an affinity similar to that of WT mouse albumin (Fig. S14 c-g, Table 1), and consequently circulated for an extended time period in WT mice (Fig. S15). Thus, despite the cross-species challenge, we compared the activity of rFVIIa-QMP with that of NovoSeven® in hemophilia B mice (expressing mouse FcRn). While the activity of rFVIIa-QMP in mouse plasma was still detectable after 72 hours, the activity in plasma from mice given rFVIIa was undetectable already after 6 hours (Fig. 7d). Lastly, we determined the plasma half-life of the fusions in the human FcRn transgenic mice expressing albumin. From the clearance curves, the advantage of the QMP mutations for enhanced pH dependent human FcRn binding was revealed, as a half-life of strikingly 2.9 days was measured for rFVIIa-QMP compared with only 0.8 days for the rFVIIa-WT fusion (Fig. 7e). Thus, the use of QMP as a carrier for rFVIIa extends its plasma half-life by almost 4-fold without compromising its therapeutics properties.

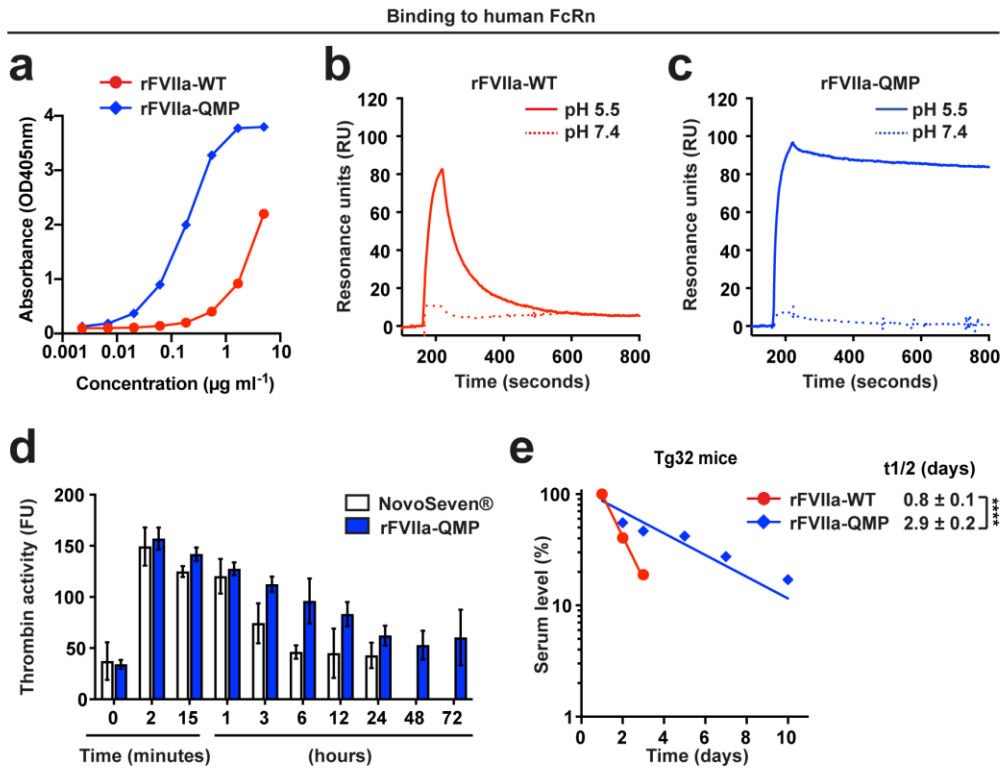

497

498 **Figure 7 | rFVIIa-QMP binds strongly to hFcRn at acidic pH and shows extended *in***
499 ***vivo* half-life.** (**a**) ELISA showing binding of rFVIIa fused to albumin WT (red) or QMP
500 (blue) to human FcRn at pH 5.5. The numbers represent the mean ± s.d. of duplicates from
501 one representative experiment. (**b-c**) SPR sensorgrams showing binding of 1000 nM
502 monomeric human FcRn injected over immobilized (~500 RU) rFVIIa-WT (b) or rFVIIa-
503 QMP (**c**) at pH 5.5 (—) or pH 7.4 (·····). Injections were performed with a flow rate of 40 µl
504 min^{-1} at 25°C. (**d**) By-passing activity measured through thrombin generation assays on
505 plasma collected from hemophilia B mice that were given 0.5 mg kg^{-1} NovoSeven® (white
506 bars) or 1 mg kg^{-1} rFVIIa-QMP (blue bars). The values represent the mean ± s.d. of 5 mice.
507 (**e**) Elimination curves of rFVIIa-WT (red) and rFVIIa-QMP (blue) in human FcRn
508 transgenic mice (n=5) that received 1 mg kg^{-1} via i.v. injection. The serum levels are
509 presented as percentage remaining in the circulation compared to that measured 1 day after
510 injection. Mean β-phase half-lives (T1/2)± S.D. are shown in days. FU, fluorescence

units. ****p < 0.0001 by unpaired T-test. Elimination curves of rFVIIa-WT (red) and rFVIIa-QMP (blue) in human FcRn transgenic mice that received 1 mg kg^{-1} via i.v. injection. The serum levels are presented as percentage remaining in the circulation compared to that measured 1 day after injection.

Discussion

It is well established that FcRn can shuttle IgG and IgG-containing complexes across cellular barriers *in vitro* (*9, 11, 50-54*). This principle has been confirmed *ex vivo,* in a placental transfer model system (*5, 55*), and *in vivo* over epithelial barriers (*7, 10, 12*). In the present study we confirm by immunohistochemistry that FcRn is expressed in normal human mucosal epithelial tissues, as in agreement with previous studies (*6-9, 15*), which suggest that FcRn may be targeted at mucosal epithelial barriers for delivery of drugs in humans.

Only two studies have so far experimentally investigated whether albumin can be shuttled across polarized cells. In both cases the MDCK model cell line was used that either over-expresses rat (*56*) or human FcRn (*57*). In one study, radiolabeled rat IgG was shown to be efficiently transcytosed in a rat FcRn-dependent manner, whereas rat albumin was not (*56*). In contrast, using human FcRn-expressing MDCK cells, human albumin was transcytosed in a receptor-dependent manner (*57*).

Here, we demonstrate that human albumin is indeed transcytosed across human epithelial cells expressing endogenous FcRn, and that efficient transcytosis requires receptor binding and an endosomal pH gradient. Importantly, we show that both albumin and IgG can be transcytosed in the presence of the other ligand, and that albumin is more efficiently transported than IgG. The reason for this is unknown, but it may relate to differences in stoichiometry. While homodimeric IgG can bind two FcRn molecules, one to each side of the Fc with equal affinity (*58*), albumin has only one binding site for the receptor (*34, 44, 46*). Despite that it is well documented that both ligands can engage the receptor simultaneously (*30, 31*), it is not clear if differences in stoichiometry may affect how FcRn is transporting the ligands within and across cell layers. Notably, it has been shown that heterodimeric IgG Fc, with only one functional FcRn binding site, is less well transported across intestinal epithelial barriers in neonatal mice and is also cleared faster from blood than WT IgG Fc (*58*). Similar

observations have been made in an *in vitro* transcytosis study (*56*). In addition, it is interesting that features of the antibody variable domains, such as hydrophobicity and charge patches, have been demonstrated to have a major influence on pharmacokinetic parameters, which has been linked to both FcRn-dependent and independent factors (*59-61*). Thus, it is not unlikely that IgG antibodies with distinct Fab features may also be transcytosed differently.

Interestingly, 50% reduction in transport was measured for an albumin variant (KAHQ) that does not bind FcRn, which was also the case when transport of WT albumin measured in the presence of a monoclonal antibody that blocks the albumin binding site on the receptor. This was in line with the *in vivo* data showing reduced transport of the non-binder KAHQ compared with WT albumin in human FcRn transgenic mice, and the fact that there were no differences in transport between WT and KAHQ in mice lacking expression of the receptor. Moreover, despite that trans-epithelial transport was reduced in the absence of FcRn, there were still some transport of albumin. This suggests that there are other mechanisms at play that also contribute to albumin uptake and transport. One possibility is that the megalin-cubilin complex is involved, as the complex has been shown to orchestrate transport of albumin together with FcRn in the kidneys (*62, 63*). In addition, cubilin may be expressed independently of megalin, as shown in human ileum tissue (*64*). Nevertheless, transcytosis of albumin was most efficient in the presence of FcRn. The involvement of FcRn was further confirmed by showing that KP, which enhances receptor binding and serum half-life (*38*), was transported better in both directions across the cell layers than the WT.

These encouraging *in vitro* data motivated design of a human albumin variant with transcytosis ability beyond that of KP, as such a variant could potentially be utilized as carriers for transmucosal delivery of protein-based biologics. To do so, we inspected our docking model of the FcRn-albumin complex (*44*) and selected two residues (E505 and

T527) to be targeted by mutagenesis (E505Q and T527M) (Fig. S16) that were combined with the KP mutation previously reported to enhance FcRn binding (*38*). It is remarkable that QMP gained 180-fold improved binding to FcRn with only minimal increase in binding at neutral pH. In fact, the best engineered IgG Fc with extended half-life published so far, has 11-fold improved binding at acidic pH, while variants with stronger FcRn binding at acidic pH, also bind at physiological pH, disrupting both transcytosis and recycling (*65-68*). When tested in Transwell, we found that QMP was transported more efficiently than the KP mutant. Importantly, QMP showed more favourable FcRn binding and transport properties beyond that of engineered human albumin variants reported by others (*46*, *47*). Thus, QMP was chosen as the lead for *in vivo* studies.

A preferred route for delivery of biologics is needle-free administration across mucosal barriers, but uptake and transcellular delivery must be efficient, cost-effective and practical. Based on our promising *in vitro* data, we aimed to overcome inefficient delivery at epithelial barriers by targeting the FcRn-transcytotic pathway using human albumin. To test this possibility, we took advantages of *state-of-the-art* mice transgenic for human FcRn, as we have shown that there are large cross-species differences in FcRn binding that exclude the use of conventional mice for studies of human albumin (*38*, *40*, *69*). By i.n. administration of equal amounts of the WT and KAHQ variants, we confirmed *in vivo* that FcRn was required for optimal uptake and that more of the WT reached the blood and persisted for a longer time than the mutant with abolished FcRn binding. Estimates revealed that roughly 25% of WT albumin reached the blood 24 hours post i.n. administration, and likely 60-70% in total, considering that 1/3 is present in blood and 2/3 extravascularly (*70-72*). In accordance with this, transport of WT albumin was reduced to that of KAHQ in mice lacking FcRn.

Initially, we found that the blood levels of QMP were similar to that of WT, which was explained by lack of competition, as the mice did not express mouse albumin. In fact, both

mice and humans have 20-50 mg/ml of albumin in blood that will compete with injected albumin-based drugs for binding to FcRn. When we repeated the experiment in mice pre-loaded with WT human albumin, 3-fold more of the QMP was taken up and reached the blood compared to the WT after 24 hours. Thus, the effect of engineering for improved pH dependent FcRn binding becomes apparent only when engineered albumin is competing for receptor binding. This observation is very important to consider when choosing an *in vivo* model for testing of human albumin fused biologics. Thus, for the half-life studies, during which the level of WT and engineered albumin was measured over an extended period of time, human FcRn transgenic mice expressing albumin was chosen. Since mouse albumin binds strongly to human FcRn (*38, 40*), these mice have high endogenous levels that compete with the injected variants for binding to the receptor, and as such mimics a natural situation.

Moreover, we extended the study to include an anti-VEGF scFv fragment N-terminally fused to WT or QMP. This scFv fragment, brolucizumab, has shown promising results in two phase III clinical trials for treatment of neovascular age-related macular degeneration, a leading cause of blindness (*73*). The scFv-fusions were administered i.n. to mice pre-loaded with WT albumin, and over 4-fold more of the QMP variant was detected in blood 24 hours after administration, corresponding to an estimated 10%, taking into account the blood-extracellular space distribution. In this study, albumin variants were simply given by adding a drop of the solution i.n., which entered the lower airways.

Fusion to albumin is an increasingly utilized strategy to improve the pharmacokinetics of short-lived therapeutics. Two products recently entered the market; Tanzeum®/Eperzan®, which is an albumin fusion of glucagon-like peptide 1 used for treatment of type 2 diabetes (*74*), and IDELVION®, which is a fusion of recombinant coagulation factor IX used to treat haemophilia (*75*). These WT human albumin-fused drugs are injected subcutaneously (Tanzeum®/Eperzan®) or intravenously (i.v.) (IDELVION®), once weekly or up to once

every second week, respectively. The same strategy has also been explored for rFVIIa, but although fusion to albumin extends the half-life in rodents by 6-7-fold (*76*), it is still unfavorably short. Importantly, these fusions are built on WT human albumin, which once injected, compete with the abundant endogenous albumin for receptor binding. For this reason, albumin designed for improved FcRn binding should confer a competitive advantage. Indeed, the QMP variant showed considerably extended *in vivo* half-life, far beyond that of other albumin variants described (*38, 46*), a phenotype that was solely due to improved pH dependent FcRn engagement. Consequently, fusion of rFVIIa to QMP resulted in almost 4-fold longer half-life than when fused to the WT. Thus, QMP should be attractive as a fusion partner to any therapeutic peptide or protein of interest with short serum persistence, and it may be utilized for efficient delivery of biologics across mucosal barriers. Importantly, there were no sign of immunogenicity of neither WT human albumin nor QMP in the mouse models used, and both were still detected in the blood after more than 50 days in human FcRn transgenic mice lacking endogenous albumin, which strongly suggests that they are well tolerated.

MATERIALS AND METHODS

Study design. The objective of this study was to engineer human albumin for improved FcRn binding that enhances cellular transport properties *in vitro* and *in vivo* in human FcRn transgenic mice. Furthermore, as albumin and IgG bind FcRn in the same pH-dependent manner, direct comparison of the two ligands was done both *in vitro* and *in vivo*. For studies using HERA and transwell assays, sample size was determined based on previous studies and experience measuring transport of IgG. For mice studies, 3-6 mice per group were used, which is based on experience and is a standard number used for determination of IgG half-life *in vivo*. For transwell studies, experiments where obvious leakage were detected from one chamber to the other were excluded from the datasets. Leakage was measured when the concentration of the opposite chamber was as high as that of the sample-adding chamber. Binding studies and cellular assays were done at least three times. Due to animal welfare, animal studies were not replicated more than twice. In ELISA, HERA and Transwell assays, the order of which analyte to be added in each well was random. Occasionally, mice from different groups were mixed together and numbered that were tracked back during analysis. When available, investigators administrated the analyte to mice without knowing the content.

T84 transcytosis assay. The human epithelial cell line T84 (ATCC) was maintained in Dulbecco`s modified Eagles Medium DMEM/F-12 medium (1:1) (Invitrogen), supplied with 20% heat inactivated fetal bovine serum, 2 mM L-glutamine, 50 U ml^{-1} streptomycin and 50 U ml^{-1} penicillin (all from Bio-Whittaker). The cells were incubated at 37^{o}C in a humidified 5% CO_2, 95% air incubator. Transwell filters (1.12 cm^2) with collagen-coated polytetrafluoroethylene (PTFE) membrane and 0.4 μm pore size (Corning Costar) were incubated ON in growth medium before 1.0 x10^6 cells were seeded in each well. Transepithelial electrical resistance (TEER) was measured daily using a MILLICELL-ERS volt-ohm meter (Millipore). The cells were cultured for 4-6 days before reaching a TER value

686 of 1,000-1,500 $\Omega \times cm^2$. Growth medium were exchanged daily. Prior to experiments, the T84
687 monolayers were washed and incubated for 1 hour in Hank`s balanced salt solution
688 (Invitrogen). 500 µl albumin (300 nM) or GST fused variants (300 nM) were added to the
689 apical or basolateral side followed by sampling of 400 µl of medium at 0 and 4 hours from
690 the opposite reservoirs. When measuring albumin transport, cells were also treated with either
691 Bafilomycin A1 (0.1 µM) (AH Diagnostics), human IgG1 (36,000-300 nM) (Infliximab,
692 Roche Diagnostics), ADM31 (300 nM), DVN24 (300 nM) (*77*) or mouse IgG2b (300 nM) 20
693 min prior and during the experiments. For measurement of IgG1 transport, 500 µl of human
694 IgG1 (300 nM) were added to the apical side followed by sampling of 400 µl of medium at 0
695 and 4 hours from the basolateral reservoir. Cells were also treated with bafilomycin A1 (0.1
696 µM) (AH Diagnostics) or albumin (4,800-300 nM) 20 min before and during experiments
697 measuring human IgG1 transport.
698 **Coagulant activity of rFVIIa variants.** Prothrombin time-based coagulation assays were
699 performed as described (*78*). Briefly, FVII-depleted human plasma (Hemosil, Instrumentation
700 Laboratory, Lexington, MA, USA) was supplemented with titrated amounts of fusion
701 proteins, and coagulation times were measured on an ACLTOP700 instrument
702 (Instrumentation Laboratory) upon addition of the coagulation activator RecombiPlasTin 2G
703 (HemosIL) and $CaCl_2$.
704 **Thrombin generation assay.** The by-passing activity of rFVIIa variants was evaluated in
705 commercially-available FVIII-deficient human plasma (George King Bio-Medical Inc) as
706 well as in plasma samples from haemophilia A patients with high-titers of anti-FVIII
707 inhibitors. Patients gave informed consent to conduct these studies. Specifically, plasma was
708 supplemented with rFVIIa variants (7-3.5 µg ml^{-1}) diluted in 20 mM Hepes, 150 mM NaCl,
709 0.1% PEG-8000, pH 7.4. Coagulation was triggered by the PPP-Reagent LOW
710 (Thrombinoscope, Stago) diluted in 20 mM Hepes, 150 mM NaCl, 5 mM $CaCl_2$, 0.1 % PEG-

8000, pH 7.4, added with MP-Reagent (1 μM; Thrombinoscope) as source of phospholipids. The generation of thrombin was measured after addition of a thrombin-specific fluorogenic substrate (Benzoyl-Phe-Val-Arg-AMC, 400 μM; Thrombin Substrate III, EMD Biosciences Inc) as fluorescence emission (Relative Fluorescence Units, RFU; 360 nm excitation, 465 nm emission) over time at 37°C on a microplate fluorometer (Fluoroskan Ascent FL, Thermo Fisher Scientific) (*79*). Novoseven® (3-1.5 μg ml^{-1}) was exploited as external control. Typical bell-shaped curves were obtained by extrapolating the first derivative of raw data as a function of time.

***In vivo* studies.** HB-balb/c mice (male, 8-12 weeks, 5 mice/group, bread in-house and the parental strain was a kind gift from prof. Darrell Stafford, University of North Carolina at Chapel Hill, United States) were injected retro-orbitally with 0.5 mg kg^{-1} of rFVIIa or 1 mg/kg of the rFVIIa fusions to achieve a circulating concentration of 100 nM. Blood samples were obtained retro-orbitally (from the opposite eye) using non-heparinized natelson tubes into 3.8% sodium citrate (1/10 final volume) at 0-2-15 minutes and 1, 3, 12, 24, 48 and 72 hours post injection. Collected blood was centrifuged at 4°C for 10 minutes at 10,000 RCF and the supernatant plasma was snap-frozen onto dry ice. The by-passing activity in plasma was evaluated by thrombin generation assays, essentially as described above with only slight modifications. Briefly, 25 μl of plasma were mixed with 15 μl of dilution buffer (20 mM Hepes, 150 mM NaCl, 0.1% PEG-8000, pH 7.4) and a mixture of the trigger Innovin (Dade Innovin, Siemens Healthcare) and 4 μM phospholipids. Thrombin generation was measured over time at 33°C upon addition of the thrombin fluorogenic substrate. Institutional approval was obtained from the Animal Care and Use Committee at the Children's Hospital of Philadelphia for mouse studies.

Half-life studies. The half-life studies were performed in Balb/c mice, homozygous FcRn KO mice (B6.129X1-Fcgrt tm1Dcr/Dcr; The Jackson Laboratory, Bar Harbor, ME),

homozygous Tg32 alb KO mice (B6.Cg-Alb^{em12Mvw} Fcgrt^{tm1Dcr} Tg(FCGRT)32Dcr/MvwJ, The Jackson Laboratory) and hemizygous Tg32 mice (B6.Cg-Fcgrt tm1Dcr Tg(FCGRT)32Dcr/ DcrJ; The Jackson Laboratory. Balb/c mice (female, 9-10 weeks, 3 mice/group) received 2 mg kg^{-1} of rFVIIa-WT or rFVIIa-QMP in 5 ml kg^{-1} 1x PBS by i.v. injection. FcRn KO mice (female, 8 weeks, 5 mice/ group) received 1 mg kg^{-1} of albumin (WT, KAHQ and QMP) in 5 ml kg^{-1} 1x PBS by i.v. injection. Blood (25 µl) was drawn from the saphenous vein at 24, 30, 35, 48, 54 and 72 hours (Balb/C) or at 24, 30, 48 and 72 hours (FcRn KO) post injection using heparinized micro capillary pipettes and maintained on ice until centrifugation at 17000 x g for 5 min at 4°C. Plasma was isolated and stored at -20°C until analysis. The studies were carried out at the Department of Pharmacology, Oslo University Hospital, Rikshospitalet. The experiment and procedures used were approved by the Norwegian Animal Research Authority and performed in accordance with the approved guidelines and regulations. Tg32 alb KO mice (male and female, 8-10 weeks, 5 mice/group) received 3.2 mg kg^{-1} of albumin (WT, KAHQ, KP and QMP) on day 0, and 1x PBS or 1 mg ADM31 on day 64, each in 20 ml kg^{-1} 1x PBS by i.p. injection. Tg32 mice (male, 7-8 weeks, 5 mice/group) received 1 mg kg^{-1} of albumin (WT, KAHQ, KP and QMP) or albumin-rFVIIa fusions (WT and QMP) in 1x PBS by i.v. injection. Blood (25 µl) was drawn from the retro-orbital sinus at 1, 8, 14, 20, 30, 45, 58, 64, 68 and 71 days (Tg32 alb KO) or 1, 2, 3, 5, 7, 10, 12, 16, 19 and 23 days (Tg32) post injection of the albumin variants. The blood samples were mixed with 1 µl 1% K3-EDTA and maintained on ice until centrifugation at 17000 x g for 5 min at 4°C. Plasma was isolated and diluted 1:10 in 50% glycerol/PBS solution and stored at -20°C until analysis. The studies were carried out at The Jackson Laboratory (JAX Service, Bar Harbor, ME), in accordance with guidelines and regulations approved by the Animal Care and Use Committee at The Jackson Laboratory. To quantify the amount of the rFVIIa fusions in plasma from Balb/c mice (diluted 1:50 in PBSTM), an anti-FVII/anti-HSA ELISA

was used as described above. To quantify the amount of albumin with or without the rFVIIa fusion in plasma from Tg32 mice (diluted 1:200 in PBSTM), a two-way anti-human albumin ELISA was used as described above. The plasma concentration was presented as percentage remaining in the circulation at different time points post injection compared to the concentration on day 1 (100%). The β-phase half-life was calculated using the formula: t1/2 = log 0.5/(log Ae/A0) × t, where t1/2 is the half-life of the human albumin variant evaluated, Ae is the concentration remaining, A0 is the concentration on day 1 and t is the elapsed time.

Pulmonary delivery studies. Homozygous Tg32 alb KO mice (B6.Cg-Alb^{em12Mvw} Fcgrt^{tm1Dcr} Tg(FCGRT)32Dcr/MvwJ, The Jackson Laboratory) and homozygous FcRn KO mice (B6.129X1-Fcgrt tm1Dcr/Dcr; The Jackson Laboratory) were used for i.n. delivery studies. A mix of female and male mice (Tg32 alb KO, 6-8 weeks, 5 mice/group) were anesthetized by i.p. injection of Zoletil mix. When sedated, 10µl of albumin or IgG1 diluted in PBS were given to each nostril followed by breathing in while lying on their backs. Specifically, 1 mg kg^{-1} albumin (WT, KAHQ or QMP) and 2.24 mg kg^{-1} IgG1 was given to each mouse. Blood was collected by puncture of the saphenous vein and collected using heparinized micro capillary pipettes after 2, 4, 8, 12, 24, 96, 144, 168, 336, 504 and 672 hours for albumin as well as 4, 8, 24 and 144 hours for IgG1.

For i.n. delivery studies with applied competition, Tg32 alb KO mice (females and males, 8 weeks, 3-6 mice/group) were pre-loaded with human albumin or human IgG (both 250 mg kg^{-1}) 48 hours before i.n. delivery of biotinylated albumin (WT, KAHQ or QMP, 1 mg kg^{-1}) or IgG1 (2.24 mg kg^{-1}), following blood samples after 4, 8, 24, 96, 168 and 360 hours (albumin) or after 4, 8, 24, 30, 48 hours (albumin and IgG1). scFv-albumin fusions (WT or QMP, 3.2 mg kg^{-1}) as well as a control Fab fragment (0.7 mg kg^{-1}) were given in the same manner as above using applied competition and blood withdrawal as above after 4, 8 and 24 hours.

For i.n. delivery studies performed in mouse FcRn KO mice (females, 8 weeks, 6 mice/group), mice were given 1 mg kg^{-1} of albumin (WT, KAHQ and QMP), followed by blood samples after 4, 8, 24, 30 and 48 hours. In addition, FcRn KO mice (females, 8 weeks, 3 mice/group) were given 1 mg kg^{-1} of albumin and 2.24 mg kg^{-1} IgG1, followed by blood withdrawal as above after 4, 8 and 24 hours. Sera from mice was isolated by centrifugations for 5 minutes at 17000 x g for 5 min at 4°C and stored at -20 after isolation.

Animals were housed under minimal disease conditions at Oslo University Hospital, Oslo, Norway. All animal experiments were approved by the National Committee for Animal Experiments (Oslo, Norway). Quantification of the amount of albumin, IgG1, Fab, biotinylated albumin or scFv-albumin fusion variants in sera was done by seven serial dilutions (1:2) of serum (diluted 1:50 in PBSTM), a two-way ELISA using anti-albumin antibodies, anti-hIgG Fc antibodies, anti-kappa light chains antibodies, protein L as well as BSA-NIP, neutravidin and recombinant VEGF as described above.

Analytical FcRn affinity chromatography. Analysis was performed using an ÄKTA FPLC instrument (GE Healthcare) and a human FcRn coupled affinity column (Roche), as previously described (*32, 45*). Briefly, 50 µl of the albumin variants (2 mg ml^{-1}) were injected and eluted by a linier pH gradient from pH 5.5-8.8 within 110 min using 20 mM MES buffer, 140 mM NaCl pH 5.5 and 20 mM Tris, 140 NaCl, pH 8.8 as eluents. To determine the elution pH as a function of retention time, the pH was monitored by a pH detector (GE Healthcare) connected to the ÄKTA FPLC instrument.

Structural analysis. Coordinates were retrieved from the protein data bank data base: crystal structure of human albumin at 2.5 Å (PDB code 1bm0), and the co-crystal structure of human FcRn in complex with WT human albumin (PDB code 4N0F) (*34*) and HSA13 (PDB code 4k71) (*46*). The docking model of human FcRn in complex with human albumin has been described (*44*). The structures were inspected using PyMOL (Schrodinger Inc.).

Statistical analysis. Data are presented as means ± SD or SEM as described in the figure legends. Statistical analysis was done using GrapPad Prism 8 software by unpaired T-test or one-way ANOVA test (Dunnett`s). *p <0.05, **p < 0.01, ***p < 0.001, ****p < 0.0001, ns: not significant p >0.05.

Acknowledgements: We are grateful to Sathiaruby Sivaganesh for excellent technical assistance, Martin B. McAdam for production of mIgG2b, Hanna Noordzij for conjugating ADM31 Fab to Alexa 647, Tor Kristian Andersen for performing the i.v. injections in Balb/c mice, Arnar Gudjonsson for performing the i.v. injections in FcRn KO mice and prof. Giancarlo Castaman for providing plasma samples from haemophilia A patients with high-titer inhibitors. We thank Dr. Wayne I. Lencer for (Boston Children's Hospital, Harvard Medical School and Harvard Digestive Diseases center) for the HMEC1 cell line stably expressing HA-hFcRn-EGFP. **Funding:** This work was supported in part by the Research Council of Norway through its Center of Excellence funding scheme (project no. 179573). J.T.A. and J.N. were supported by the Research Council of Norway (Grant no. 230526) and South-Eastern Norway Regional Health Authority (Grant no. 40018). M.B. was supported by the Research Council of Norway through its program for Global Health and Vaccination Research (GLOBVAC) (Grant no. 143822) and program for biotechnology and innovation (BIOTEK2021) (Grant no. 267606). S.F. was supported by the Research Council of Norway (grant no. 251037/F20). H.E.L. was supported by the South-Eastern Norway Regional Health Authority (grant no. 40109), H.E.L, and T.G.T. in part by Dr. Jon S Larsens Foundation. A.B. and M.P. were supported by the Bayer Early Career Investigator Award (Bayer Hemophilia Award Program) 2018. A.B. and M.P. would also like to acknowledge the support provided by PFIZER EuroAspire projects WI199905 (A.B.) and WI193137 (M.P.). **Author contributions:** M.B., M.F., J.N., K.M.K.S., T.T.G., H.E.L., I.S., M.P., R.M.C., B.D., M.C.M., A.B. and J.T.A. designed research; M.B., M.F., J.N., K.M.K.S., R.J.D., T.T.G.,

H.E.L, E.S.B., S.F., A.G., J.W., L.S.H., G.J.C., T.S., T.E.M., S.L. and A.B. performed research; M.B., M.F., J.N., K.M.K.S., T.T.G., H.E.L., S.F., A.G., E.S.B., B.D., I.S., M.P., D.C.R., R.M.C., A.B., and J.T.A. analyzed data; M.B., M.F., J.N., K.M.K.S., A.B. and J.T.A. wrote the manuscript. All authors revised and approve the final version of the manuscript. **Competing interests:** I.S., J.T.A., M.B. and K.M.K.S. are co-inventors on pending patent applications, which are entitled 'Albumin Variants and uses thereof' and relate to the data described in this paper. The remaining authors have no competing financial interest to declare. M.C.M. is member of Bayer and Novartis advisory boards. **Data and materials availability:** The datasets generated during and/or analyzed during the current study are available from the corresponding author on reasonable request.

References

1. M. M. France, J. R. Turner, The mucosal barrier at a glance. *Journal of Cell Science,* (2017).
2. M. Goldberg, I. Gomez-Orellana, Challenges for the oral delivery of macromolecules. *Nat Rev Drug Discov* **2**, 289-295 (2003).
3. R. Halliday, Prenatal and postnatal transmission of passive immunity to young rats. *Society, The Royal Society, Royal Sciences, Biological* **144**, 427-430 (1955).
4. C. M. Story, J. E. Mikulska, N. E. Simister, A major histocompatibility complex class I-like Fc receptor cloned from human placenta: possible role in transfer of immunoglobulin G from mother to fetus. *The Journal of experimental medicine* **180**, 2377-2381 (1994).
5. M. Firan *et al.*, The MHC class I-related receptor, FcRn, plays an essential role in the maternofetal transfer of gamma-globulin in humans. *International immunology* **13**, 993-1002 (2001).
6. Z. Li *et al.*, Transfer of IgG in the female genital tract by MHC class I-related neonatal Fc receptor (FcRn) confers protective immunity to vaginal infection. *Proceedings of the National Academy of Sciences of the United States of America* **108**, 4388-4393 (2011).
7. G. M. Spiekermann *et al.*, Receptor-mediated Immunoglobulin G Transport Across Mucosal Barriers in Adult Life: Functional Expression of FcRn in the Mammalian Lung. *Journal of Experimental Medicine* **196**, 303-310 (2002).
8. E. J. Israel *et al.*, Expression of the neonatal Fc receptor, FcRn, on human intestinal epithelial cells. *Immunology* **92**, 69-74 (1997).

9. B. L. Dickinson *et al.*, Bidirectional FcRn-dependent IgG transport in a polarized human intestinal epithelial cell line. *The Journal of clinical investigation* **104**, 903-911 (1999).
10. M. Yoshida *et al.*, Human Neonatal Fc Receptor Mediates Transport of IgG into Luminal Secretions for Delivery of Antigens to Mucosal Dendritic Cells. *Immunity* **20**, 769-783 (2004).
11. S. Foss *et al.*, Enhanced FcRn-dependent transepithelial delivery of IgG by Fc-engineering and polymerization. *Journal of Controlled Release* **223**, (2016).
12. M. Yoshida *et al.*, Neonatal Fc receptor for IgG regulates mucosal immune responses to luminal bacteria. *The Journal of clinical investigation* **116**, 2142-2151 (2006).
13. A. J. Bitonti, J. a. Dumont, Pulmonary administration of therapeutic proteins using an immunoglobulin transport pathway. *Advanced drug delivery reviews* **58**, 1106-1118 (2006).
14. S. Vallee *et al.*, Pulmonary administration of interferon Beta-1a-fc fusion protein in non-human primates using an immunoglobulin transport pathway. *Journal of interferon & cytokine research : the official journal of the International Society for Interferon and Cytokine Research* **32**, 178-184 (2012).
15. A. J. Bitonti *et al.*, Pulmonary delivery of an erythropoietin Fc fusion protein in non-human primates through an immunoglobulin transport pathway. *Proceedings of the National Academy of Sciences of the United States of America* **101**, 9763-9768 (2004).
16. J. a. Dumont *et al.*, Delivery of an erythropoietin-Fc fusion protein by inhalation in humans through an immunoglobulin transport pathway. *Journal of aerosol medicine : the official journal of the International Society for Aerosols in Medicine* **18**, 294-303 (2005).

17. S. C. Low, S. L. Nunes, a. J. Bitonti, J. a. Dumont, Oral and pulmonary delivery of FSH-Fc fusion proteins via neonatal Fc receptor-mediated transcytosis. *Human reproduction (Oxford, England)* **20**, 1805-1813 (2005).

18. L. Lu. (2011).

19. L. Ye, R. Zeng, Y. Bai, D. C. Roopenian, X. Zhu, Efficient mucosal vaccination mediated by the neonatal Fc receptor. *Nature biotechnology* **29**, 158-163 (2011).

20. Z. Gan, S. Ram, R. J. Ober, E. S. Ward, Using multifocal plane microscopy to reveal novel trafficking processes in the recycling pathway. *Journal of cell science* **126**, 1176-1188 (2013).

21. R. J. Ober, C. Martinez, C. Vaccaro, J. Zhou, E. S. Ward, Visualizing the site and dynamics of IgG salvage by the MHC class I-related receptor, FcRn. *Journal of immunology* **172**, 2021-2029 (2004).

22. E. S. Ward *et al.*, From sorting endosomes to exocytosis: association of Rab4 and Rab11 GTPases with the Fc receptor, FcRn, during recycling. *Molecular biology of the cell* **16**, 2028-2038 (2005).

23. E. S. Ward, Evidence to support the cellular mechanism involved in serum IgG homeostasis in humans. *International Immunology* **15**, 187-195 (2003).

24. R. J. Ober, C. Martinez, X. Lai, J. Zhou, E. S. Ward, Exocytosis of IgG as mediated by the receptor, FcRn: an analysis at the single-molecule level. *Proceedings of the National Academy of Sciences of the United States of America* **101**, 11076-11081 (2004).

25. P. Prabhat *et al.*, Elucidation of intracellular recycling pathways leading to exocytosis of the Fc receptor, FcRn, by using multifocal plane microscopy. *Proceedings of the National Academy of Sciences of the United States of America* **104**, 5889-5894 (2007).

26. H. P. Montoyo *et al.*, Conditional deletion of the MHC class I-related receptor FcRn reveals the sites of IgG homeostasis in mice. *Proceedings of the National Academy of Sciences of the United States of America* **106**, 2788-2793 (2009).
27. H. L. Spiegelberg, B. G. Fishkin, The catabolism of human γG immunoglobulins of different heavy chain subclasses. 3. The catabolism of heavy chain disease proteins and of Fc fragments of myeloma proteins. *Clinical and experimental immunology* **10**, 599-607 (1972).
28. T. Peters, Serum Albumin. *Advances in Protein Chemistry* **37**, (1985).
29. C. Chaudhury *et al.*, The Major Histocompatibility Complex-related Fc Receptor for IgG (FcRn) Binds Albumin and Prolongs Its Lifespan. *Journal of Experimental Medicine* **197**, 315-322 (2003).
30. J. T. Andersen, J. Dee Qian, I. Sandlie, The conserved histidine 166 residue of the human neonatal Fc receptor heavy chain is critical for the pH-dependent binding to albumin. *European journal of immunology* **36**, 3044-3051 (2006).
31. C. Chaudhury, C. L. Brooks, D. C. Carter, J. M. Robinson, C. L. Anderson, Albumin binding to FcRn: distinct from the FcRn-IgG interaction. *Biochemistry* **45**, 4983-4990 (2006).
32. A. Grevys *et al.*, A human endothelial cell-based recycling assay for screening of FcRn targeted molecules. *Nature Communications* **9**, (2018).
33. E. G. W. Schmidt *et al.*, Direct demonstration of a neonatal Fc receptor (FcRn)-driven endosomal sorting pathway for cellular recycling of albumin. *Journal of Biological Chemistry* **292**, 13312-13322 (2017).
34. V. Oganesyan *et al.*, Structural insights into neonatal Fc receptor-based recycling mechanisms. *Journal of Biological Chemistry* **289**, 7812-7824 (2014).

35. T. Peters, All about albumin. *All about albumin: Biochemistry, Genetics and Medical Applications. Academic Press*, (1996).
36. U. Kragh-Hansen, V. T. G. Chuang, M. Otagiri, Practical aspects of the ligand-binding and enzymatic properties of human serum albumin. *Biological & pharmaceutical bulletin* **25**, 695-704 (2002).
37. M. Bern, K. M. K. K. M. K. Sand, J. Nilsen, I. Sandlie, J. T. J. T. Andersen, The role of albumin receptors in regulation of albumin homeostasis: Implications for drug delivery. *Journal of Controlled Release* **211**, 144-162 (2015).
38. J. T. Andersen *et al.*, Extending serum half-life of albumin by engineering neonatal Fc receptor (FcRn) binding. *The Journal of biological chemistry* **289**, 13492-13502 (2014).
39. T. Yoshimori, A. Yamamoto, Y. Moriyama, M. Futai, Y. Tashiro, Bafilomycin A1, a specific inhibitor of vacuolar-type H+-ATPase, inhibits acidification and protein degradation in lysosomes of cultured cells. *Journal of Biological Chemistry* **266**, 17707-17712 (1991).
40. J. T. Andersen, M. B. Daba, G. Berntzen, T. E. Michaelsen, I. Sandlie, Cross-species binding analyses of mouse and human neonatal Fc receptor show dramatic differences in immunoglobulin G and albumin binding. *The Journal of biological chemistry* **285**, 4826-4836 (2010).
41. D. C. Roopenian *et al.*, Albumin-deficient mouse models for studying metabolism of human albumin and pharmacokinetics of albumin-based drugs. *mAbs* **7**, 344-351 (2015).
42. J. Nilsen, I. Sandlie, D. C. Roopenian, J. T. Andersen, Animal models for evaluation of albumin-based therapeutics. *Current Opinion in Chemical Engineering* **19**, 68-76 (2018).

43. Y. Y. Fan *et al.*, Tissue expression profile of human neonatal Fc receptor (FcRn) in Tg32 transgenic mice. *MAbs* **8**, 848-853 (2016).
44. J. T. Andersen *et al.*, Structure-based mutagenesis reveals the albumin-binding site of the neonatal Fc receptor. *Nature Communications* **3**, 1-9 (2012).
45. T. Schlothauer *et al.*, Analytical FcRn affinity chromatography for functional characterization of monoclonal antibodies. *mAbs* **5**, 576-586 (2013).
46. M. M. Schmidt *et al.*, Crystal Structure of an HSA / FcRn Complex Reveals Recycling by Competitive Mimicry of HSA Ligands at a pH-Dependent Hydrophobic Interface. *Structure* **21**, 1966-1978 (2013).
47. C. C. Changshou Gao, Xiaotao Yao, Hsa-related compositions and methods of use. (2011).
48. K. M. K. Sand *et al.*, Dissection of the neonatal Fc receptor (FcRn)-albumin interface using mutagenesis and anti-FcRn albumin-blocking antibodies. *Journal of Biological Chemistry* **289**, (2014).
49. E. Erhardtsen, Pharmacokinetics of recombinant activated factor VII (rFVIIa). *Seminars in thrombosis and hemostasis* **26**, 385-391 (2000).
50. K. M. McCarthy, Y. Yoong, N. E. Simister, Bidirectional transcytosis of IgG by the rat neonatal Fc receptor expressed in a rat kidney cell line: a system to study protein transport across epithelia. *Journal of cell science* **113**, 1277-1285 (2000).
51. I. Ellinger, M. Schwab, A. Stefanescu, W. Hunziker, IgG transport across trophoblast-derived BeWo cells : a model system to study IgG transport in the placenta. *European journal of immunology* **29**, 733-744 (1999).
52. P. J. Hornby *et al.*, Human and Non-Human Primate Intestinal FcRn Expression and Immunoglobulin G Transcytosis. *Pharmaceutical research* **31**, 908-922 (2013).

53. N. M. Stapleton *et al.*, Competition for FcRn-mediated transport gives rise to short half-life of human IgG3 and offers therapeutic potential. *Nature Communications* **2**, 599 (2011).

54. S. M. Claypool, B. L. Dickinson, M. Yoshida, W. I. Lencer, R. S. Blumberg, Functional Reconstitution of Human FcRn in Madin-Darby Canine Kidney Cells Requires Co-expressed Human 2 -Microglobulin *. *The Journal of biological chemistry* **277**, 28038-28050 (2002).

55. L. Mathiesen *et al.*, Maternofetal transplacental transport of recombinant IgG antibodies lacking effector functions. *Blood* **122**, 1174-1182 (2013).

56. D. B. Tesar, N. E. Tiangco, P. J. Bjorkman, Ligand Valency Affects Transcytosis, Recycling and Intracellular Trafficking Mediated by the Neonatal Fc Receptor. *Traffic* **7**, 1127-1142 (2006).

57. M. Pyzik *et al.*, Hepatic FcRn regulates albumin homeostasis and susceptibility to liver injury. *Proceedings of the National Academy of Sciences*, (2017).

58. Y. N. Abdiche *et al.*, The neonatal Fc receptor (FcRn) binds independently to both sites of the IgG homodimer with identical affinity. *mAbs* **7**, 331-343 (2015).

59. A. Schoch *et al.*, Charge-mediated influence of the antibody variable domain on FcRn-dependent pharmacokinetics. *Proc Natl Acad Sci U S A* **112**, 5997-6002 (2015).

60. P. F. Jensen *et al.*, Investigating the interaction between the neonatal Fc receptor and monoclonal antibody variants by hydrogen/deuterium exchange mass spectrometry. *Molecular & cellular proteomics : MCP* **14**, 148-161 (2015).

61. R. L. Kelly *et al.*, Target-independent variable region mediated effects on antibody clearance can be FcRn independent. *MAbs* **8**, 1269-1275 (2016).

62. S. Amsellem *et al.*, Cubilin is essential for albumin reabsorption in the renal proximal tubule. *J Am Soc Nephrol* **21**, 1859-1867 (2010).

63. S. Cui, P. J. Verroust, S. K. Moestrup, E. I. Christensen, Megalin/gp330 mediates uptake of albumin in renal proximal tubule. *Am J Physiol* **271**, F900-907 (1996).
64. L. L. Jensen, R. K. Andersen, H. Hager, M. Madsen, Lack of megalin expression in adult human terminal ileum suggests megalin-independent cubilin/amnionless activity during vitamin B12 absorption. *Physiol Rep* **2**, (2014).
65. W. F. Dall'Acqua, P. a. Kiener, H. Wu, Properties of human IgG1s engineered for enhanced binding to the neonatal Fc receptor (FcRn). *The Journal of biological chemistry* **281**, 23514-23524 (2006).
66. C. Vaccaro, J. Zhou, R. J. Ober, E. S. Ward, Engineering the Fc region of immunoglobulin G to modulate in vivo antibody levels. *Nature biotechnology* **23**, 1283-1288 (2005).
67. C. Vaccaro, R. Bawdon, S. Wanjie, R. J. Ober, E. S. Ward, Divergent activities of an engineered antibody in murine and human systems have implications for therapeutic antibodies. *Proceedings of the National Academy of Sciences of the United States of America* **103**, 18709-18714 (2006).
68. J. Zalevsky *et al.*, Enhanced antibody half-life improves in vivo activity. *Nature biotechnology* **28**, 157-159 (2010).
69. J. T. Andersen *et al.*, Single-chain Variable Fragment Albumin Fusions Bind the Neonatal Fc Receptor (FcRn) in a Species-dependent Manner: IMPLICATIONS FOR IN VIVO HALF-LIFE EVALUATION OF ALBUMIN FUSION THERAPEUTICS. *The Journal of biological chemistry* **288**, 24277-24285 (2013).
70. M. A. Rothschild, A. Bauman, R. S. Yalow, S. a. Berson, Tissue distribution of I131 labeled human serum albumin following intravenous administration. *Journal of Clinical Investigation* **34**, 1354-1358 (1955).

71. J. Katz, G. Bonorris, A. L. Sellers, Extravascular albumin in human tissues. *Clin Sci* **39**, 725-729 (1970).
72. W. L. Beeken *et al.*, STUDIES OF I131-ALBUMIN CATABOLISM AND DISTRIBUTION IN NORMAL YOUNG MALE ADULTS *. *Journal of Clinical Investigation* **41**, (1962).
73. P. U. Dugel *et al.*, Brolucizumab Versus Aflibercept in Participants with Neovascular Age-Related Macular Degeneration: A Randomized Trial. *Ophthalmology* **124**, 1296-1304 (2017).
74. M. S. Rendell, Albiglutide: a unique GLP-1 receptor agonist. *Expert opinion on biological therapy* **16**, 1557-1569 (2016).
75. E. Santagostino, Transforming the treatment for hemophilia B patients: update on the clinical development of recombinant fusion protein linking recombinant coagulation factor IX with recombinant albumin (rIX-FP). *Thrombosis research* **141 Suppl 3**, S5-8 (2016).
76. T. Weimer *et al.*, Prolonged in-vivo half-life of factor VIIa by fusion to albumin. *Thrombosis and haemostasis* **99**, 659-667 (2008).
77. G. J. Christianson *et al.*, Monoclonal antibodies directed against human FcRn and their applications. *mAbs* **4**, 208-216 (2012).
78. A. Branchini *et al.*, Differential functional readthrough over homozygous nonsense mutations contributes to the bleeding phenotype in coagulation factor VII deficiency. *Journal of thrombosis and haemostasis : JTH* **14**, 1994-2000 (2016).
79. E. Barbon *et al.*, An engineered tale-transcription factor rescues transcription of factor VII impaired by promoter mutations and enhances its endogenous expression in hepatocytes. *Sci Rep* **6**, 28304 (2016).

1069

1070

1071

1072

1073

1074

1075

1076

1077

1078

1079

1080

1081

1082

1083

1084

1085

1086

1087

1088

1089

1090

1091

1092

1093

Supplementary materials and methods

Confocal immunofluorescence microscopy and immunohistochemistry. T84 cells were seeded on gelatin coated glass slides (Thermo Fisher Scientific) and grown to confluent monolayers. Cells were then fixed by incubation in acetone for 10 min. The glass slides were air-dried and washed in PBS prior to staining using the anti-human FcRn monoclonal antibodies ADM31 or DVN24 (*1*). The antibodies were diluted in PBS with 1.25% bovine serum albumin to a final concentration of 5 μg ml^{-1} and incubated with T84 cells for 90 min. mIgG2b (R&D Systems) or mIgG2a (Sigma-Aldrich) antibodies with irrelevant specificity were used as isotype controls. The cells were then washed for 2 min in PBS followed by 90 min incubation with an anti-mouse IgG antibody conjugated to Cy3 (Jackson Immuno Research). Cells were incubated in a Hoechst/PBS solution to visualize nuclei and washed in dH_2O before mounting of cover glass using polyvinyl alcohol (Sigma-Aldrich). Frozen vaginal and rectum tissue sections from healthy adult humans were acquired from BioChain, whereas human small intestine tissue was obtained from pancreatic cancer patients undergoing pancreatic duodenectomy. Material analyzed was the distal part of resected small intestine (distal duodenum/proximal jejunum) from patients without metastases, who had not undergone previous treatment, and sampling was approved by the Norwegian Regional Committee for Medical Research Ethics. For staining of tissue sections, a Fab fragment of the FcRn specific ADM31 antibody was made by papain cleavage, and a mouse IgG Fab with irrelevant specificity was acquired from Rockland Immunochemicals. Both were conjugated with Alexa 647 (Molecular Probes/Life Technologies) following the manufacturer's instructions. Confocal images were acquired using an Olympus FluoView1000 microscope equipped with PlanApo 60/1.35 and PlanApo 20/1.1 oil objectives (Olympus). For live cell imaging cells were seeded on collagen coated imaging wells (MatTek Corporation) and grown to form confluent monolayers. Alexa 647 conjugated ADM31-Fab (5 μg ml^{-1}) or

Alexa 488 conjugated ZO-1 specific antibody (Life Technologies, 7.5 μg ml^{-1}) diluted in Hank`s balanced salt solution (Invitrogen) were added to the cells to visualize FcRn and tight junctions, respectively. An incubator enclosing the microscope stage allowed the temperature to be set to 37°C and CO_2 to 5%. Confocal images were acquired using an Olympus FluoView1000 inverted microscope with a PlanApo 60/1.42 oil objective (Olympus). Image acquisition was done by sequential line scanning. Images were processed using Image J (National Institute of Health) and Adobe Illustrator (Adobe Systems Inc).

ELISA. ELISA based FcRn binding to the different albumin formats was performed as previously described (*2, 3*). Transport of albumin variants or IgG1 across polarized T84 cells, as well as serum concentration of albumin formats, Fab and IgG1 in mouse sera was quantified using ELISA. Albumin, IgG1 or Fab fractions with known concentrations were used as standards. An anti-GST antibody from goat (diluted 1:2,000) (GE Healthcare), anti-human albumin antibody from goat (diluted 1:2,000) (Sigma-Aldrich), VEGF-165 (0.5 μg ml^{-1}) (Sino Biological, USA), NeutrAvidin (2 μg ml^{-1}) (Thermo Fischer), BSA-NIP (1 μg ml^{-1}), polyclonal sheep anti-human factor VII (Cedarlane) (1:2000), anti-human IgG Fc antibody from sheep (diluted 1:10,000) (in-house produced) or an ALP-conjugated anti-human kappa light chains antibody from goat (diluted 1:1,000) (Sigma-Aldrich), diluted in 1xPBS were coated in 96-well NUNC plates and incubated at 4^{o}C overnight (ON). Wells were then blocked using 200 μl 4% Skim milk (M)/PBS for 1 hour before washed 4 times with PBS/tween (T) followed by adding of titrated amounts IgG, Fab or albumin (diluted in PBSTM) in parallel with samples collected from the Transwell system or mouse sera. Followed by incubation for 1 hour at RT, the wells were washed as above. Subsequently, an HRP-conjugated monoclonal anti-human albumin antibody from mouse (Abcam) (diluted 1:5,000), ALP-conjugated polyclonal anti-human albumin antibody from goat (BETHYL) (diluted 1:4,000), an anti-human IgG Fc-ALP (Sigma-Aldrich) (diluted 1:5,000) or HRP

conjugated protein L (diluted 1:2,000) (Sigma-Aldrich) all in diluted in PBSTM, was added and incubated for 1 hour at RT. After washing as above, 100 µl TMB solution (Merck) or p-nitropenylphospate substrate (Sigma-Aldrich) was added followed by absorbance measurements at 620 nm or 405 nm, respectively, using the Sunrise spectrophotometer (TECAN). To terminate the reactions after adding TMB, 100 µl 1M HCl was added followed by absorbance measurement at 450 nm.

SPR. SPR experiments were performed on a BIAcore 3000 or T200 instrument (GE Healthcare). An amine coupling kit (GE Healthcare) was used for immobilization on CM5 chips (GE Healthcare), where albumin (6 µg ml^{-1}) and albumin fused to GST (2 µg ml^{-1}), scFv (4 µg ml^{-1}) or rFVIIa (6 µg ml^{-1}) injected in 10 mM sodium acetate at pH 5.0 (GE Healthcare), essentially as described by the manufacturer. Unreacted moieties on the chip surfaces were blocked with 1 M ethanolamine. Buffers containing 67 mM phosphate buffer, 0.15 M NaCl, 0.005% Tween 20 at pH 5.5 or 7.4 were used as running buffers. Kinetic measurements were performed by injecting serial dilutions of monomeric human FcRn (1.0-0.015 µM) or mouse FcRn (1.0-0.0315 µM) over immobilized albumin variants at pH 5.5 or 7.4, with a flow rate of 40-50 µl min^{-1} at 25°C. Kinetic rate values were calculated using the simple Langmuir 1:1 ligand binding model provided by the BIAevaluation 4.1 software or Biacore T200 Evaluation 3.0 Software (GE Healthcare). The closeness of the fit, described by the statistical value χ^2, which represents the mean square, was below 4.0 in all affinity estimations. To correct for nonspecific binding and bulk buffer effects, binding responses obtained from the control CM5 flow cells and blank injections were subtracted from each interaction curve.

Construction and production of soluble human FcRn. Soluble truncated human and mouse FcRn variants were produced as described (*4-6*). The viral stocks was a kind gift from Professor Sally Ward (University of Southampton, UK).

Construction and production of recombinant IgG formats and albumin variants. The cDNA fragment encoding full-length human albumin was cloned into a naked pcDNA3 (Invitrogen) vector (pcDNA3-albumin) for the production of unfused albumin. For construction of albumin with a C-terminal GST fusion, the cDNA segment encoding human albumin was sub-cloned in frame of a gene encoding GST from *Schistosoma japonicum* in a pcDNA3 vector containing Epstein Barr virus origin of replication (OriP) (pcDNA3-albumin-GST-OriP), as described earlier (*7*). A panel of cDNA fragments encoding albumin DIII variants (462 nt) with nucleotide mutations were ordered in pUC57 vectors from GenScript, and subsequently sub-cloned into pcDNA3-albumin or pcDNA3-albumin-GST-OriP using the restriction sites *XhoI* and *BamHI*. A *BamHI* restriction site was introduced in the albumin cDNA sequence of the vectors to allow for sub-cloning of fragments encoding DIII. Brolucizumab fused to the N-terminal end of albumin was generated by adding the cDNA encoding brolucizumab (IMGT/mAb-DB ID; 536), converted to cDNA via a human codon table (Backtranseq software) to the 5`-end of the cDNA encoding WT human albumin (GenScript). The brolucizumab-albumin fragment was subsequently sub-cloned into the vector pLNOH2-hIgG1-WT-oriP (*8*) using the BsmI/BamHI restriction sites. KAHQ and QMP mutant versions were generated by site-specific mutagenesis (GenScript) using the WT vector as template. Production of albumin formats was conducted by transient transfection of HEK293E cells using polyethyleneimine-Max (PEI-Max; MW 4000; Polysciences), as previously described (*2*). Contruction and production of human IgG1 with specificity for 4-hydroxy-5-iodo-3-nitro-phenyl acetyl (NIP) was done as described (*6, 9*). A Fab fragment specific for the peptide-MHC complex HLA-DQ2.5 with the DQ2.5-glia-α1a epitope (*10*) was constructed by sub-cloning a BsiWI/BamHI flanked synthetic gene fragment (GenScript Inc) encoding CH1 of human IgG1, the first residues of the hinge (EPKSCD, the E naturally resulting from CH1-hinge splicing) and a stop codon into the vector pLNOH2-IgG1-N297G-

oriP encoding the heavy chain of IgG1 with the 106 specificity (*10*). The vector pLNOk encoding the light chain of the 106 specificity with a human constant kappa domain has been described (*10*). The Fab fragment was produced in HEK293E cells by transient transfection using Lipofectamine 2000 as previously described (*11*).

Constructs containing rFVII fused to the N-terminal end of albumin were made by sub-cloning of cDNA encoding human albumin (corresponding to aa 25-585) into the pcDNA3 expression vector downstream of a cDNA segment encoding WT human FVII, engineered with the RKRRKR (2RKR) motif in the activation site (between the corresponding Arg152-Val153, FVII numbering) (*12*), to secure secretion of a furin-cleaved activated double-chain recombinant FVII (rFVIIa). The cDNA segment encoding this motif was introduced the QuickChange II XL Site-Directed Mutagenesis Kit (Agilent Technologies) as described (*13*). A cDNA sequence corresponding to a 32-residue glycine-serine flexible linker was inserted between the 2RKR-rFVIIa and human albumin (rFVIIa-WT) (*14, 15*). This template was used to introduce the E505Q, T527M and K573P mutations, which gave rise to rFVIIa-QMP. For production of rFVIIa-fusions, stably-expressing HEK293 cells were made as described (*15*).

Purification of albumin and rFVIIa-albumin fusions and scFv-albumin-fusions were conducted using Capture Select Human Serum Albumin affinity matrix (Invitrogen) packed in a 5ml column (Atoll GmbH) as described (*3*), while a GSTrap™ FF column (GE Healthcare) was used for purification of albumin-GST fusions as described (*9*). Site-specific biotinylation of albumin (cysteine 34) was done using EZ-link™ BMCC-Biotin (Thermo Scientific) and the conjugated fraction was isolated using a Superdex 200 Increase 10/300 GL column (GE Healthcare). 2-3 μg of each protein sample was analyzed on a 12% Bis-Tris NuPAGE SDS-PAGE gel (Invitrogen) together with Spectra™ Multicolor Broad Range

Protein Ladder (ThermoFisher). Protein concentrations were determined using a DS-11 spectrophotometer (DeNovix) before all fractions were stored at -20^{o}C.

CD spectroscopy. CD spectra were recorded using a Jasco J-810 spectropolarimeter (Jasco International) calibrated with ammonium d-camphor-10-sulfonate (Icatayama Chemicals). Measurements were performed with albumin and GST-fusions (0.1 mg ml $^{-1}$) in 10 mM PBS (pH 5.5) without NaCl added, at 25 °C using a quartz cuvette (Starna) with a path length of 0.1 cm. Each sample was scanned 5 times at 50 nm min $^{-1}$ (bandwidth of 1 nm, response time of 4 s) with wavelength range set to 190-260 nm. The data were averaged and the spectrum of a sample-free control was subtracted. Secondary structural elements were calculated using the neural network program CDNN version 2.1 and the supplied neural network based on the 33-member basis set (*16*).

Flow Cytometry. The U937 and T84 cell lines (ATCC) were stained for surface expression of CD32 and CD64 using Phycoerythrin (PE)-conjugated monoclonal antibodies diluted in PBS containing 4% FCS. The cells were subsequently fixed in 4% paraformaldehyde and gated on a FACSCalibur (BD Biosciences). Data analysis was performed using FlowJo (TreeStar). The antibodies used for staining were from Abcam: anti-CD16-PE (3G8) (ab117117), anti-CD32-PE (AT10) (ab30357), anti-CD64-PE (10.1) and mouse IgG1-PE (ICIG1) isotype control (ab911357). Unstained cells were included as control.

HERA. The assay was performed as previously described (*3*). Briefly, 7.5 × 10^{5} HMEC-1 cells stably expressing HA-hFcRn-EGFP (*17*) were seeded into 24-well plates per well (Costar) and cultured for one day in growth medium. The cells were washed twice and starved for 1 h in Hank's balanced salt solution (HBSS) (Life Technologies). WT human albumin, KP or QMP (1000 nM) diluted in 250 µl HBSS (pH 7.4) was added per well and incubated for 4 h. The medium was removed and the cells were washed five times with ice cold HBSS (pH 7.4). Growth medium supplemented with MEM non-essential amino acids

(ThermoFisher) was added and collected after 4h. To quantify the amount of HSA in the samples, a two-way anti-human albumin ELISA was used as described above.

Supplementary tables and figures

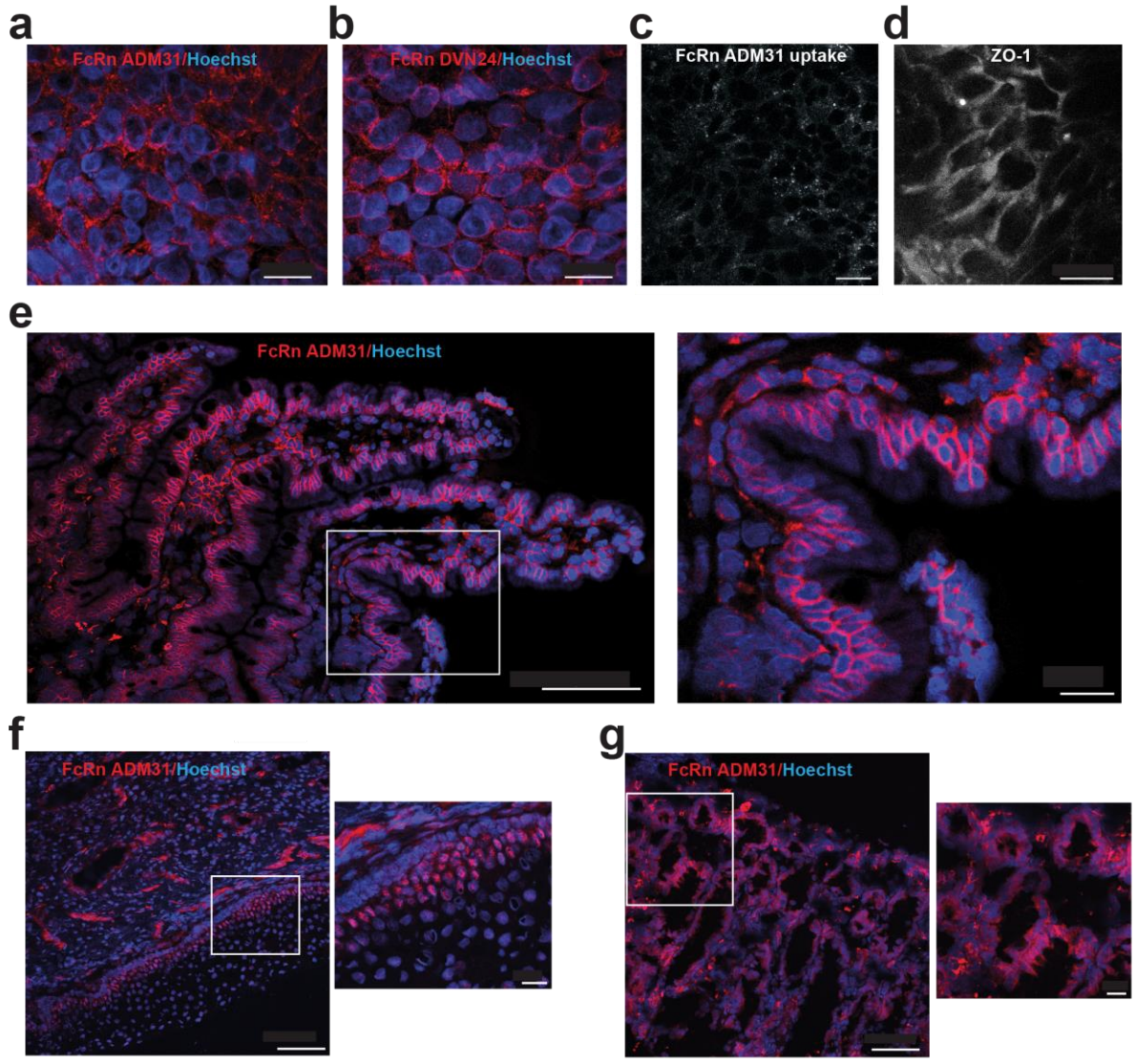

Figure S1. FcRn is expressed in human epithelial cells. T84 cells were seeded on gelatin-coated coverslips, grown to form confluent monolayers, fixed in acetone and stained with the human FcRn specific monoclonal antibodies **(a)** ADM31 and **(b)** DVN24. **(c)** The presence of FcRn in endosomes trafficking via the plasma membrane was verified by adding Alexa 647-conjugated ADM31 to live cells seeded on collagen coated imaging wells. **(d)** Formation of tight junctions was addressed by adding an Alexa 488-conjugated antibody specific for the tight junction marker ZO-1 to live T84 cells seeded on collagen coated imaging wells. To verify the presence of FcRn in epithelial cells of different tissues, acetone fixed frozen tissue

sections from **(e)** human small intestine, **(f)** vagina, and **(g)** rectum were stained with Alexa 647-conjugated ADM31. Scale bars **(a-d)** 20 µm, **(e-g)** 100 µm or 20 µm (close up).

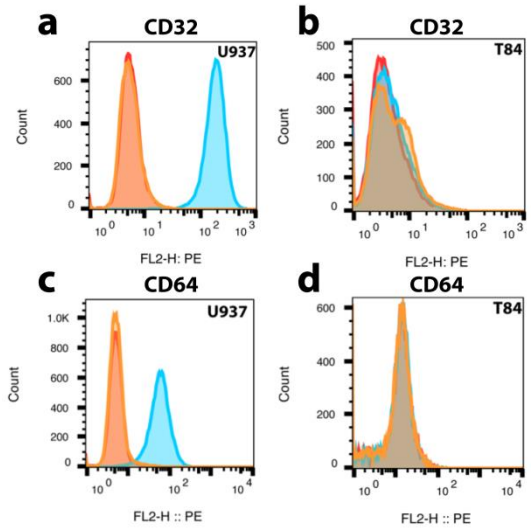

Figure S2. T84 cells do not express surface CD32 or CD64. FACS surface staining of U937 and T84 cells using phycoerythrin (PE) conjugated CD32 specific **(a-b)** and CD64 specific antibodies **(c-d)**. Unstained cells are shown in red; isotype control is shown in yellow and cells stained with anti-CD32 or anti-CD64 are shown in blue.

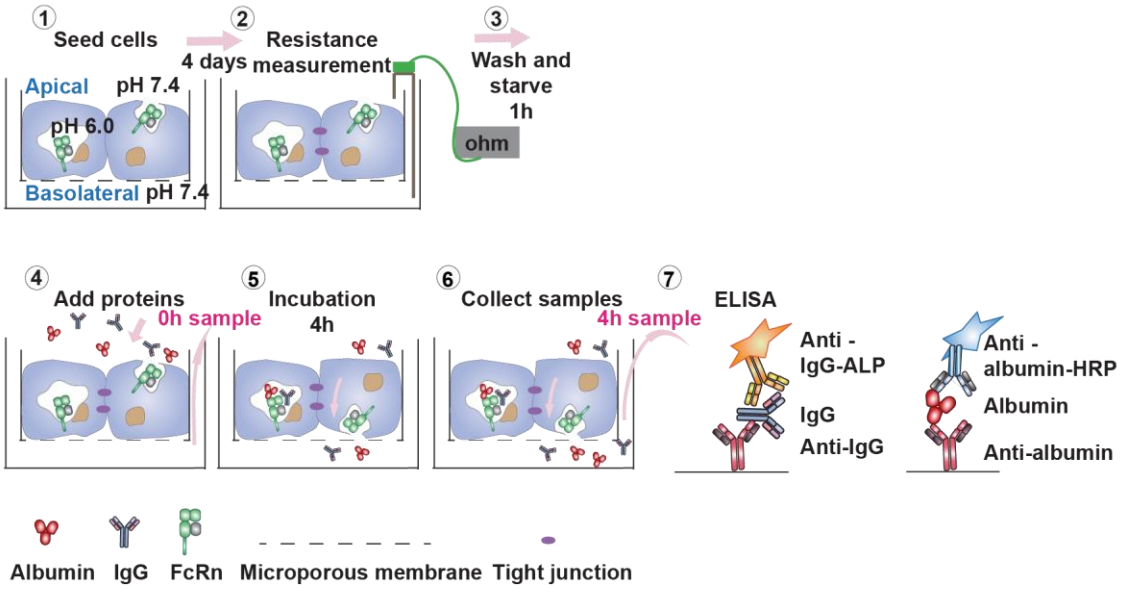

Figure S3. A schematic illustration of the transcytosis assay. T84 cells are seeded on collagen-coated Transwell filters (1) and the transepithelial resistance (TER) is measured the following days using electrodes (2). On the day of optimal TER (1,000-1,500 $\Omega \cdot cm^2$), cells are washed and incubated with HBSS for 1 hour (h) (3), followed by addition of the protein of interest (albumin and/or IgG). Samples are collected at time 0 h at the opposite side of the Transwell insert (4). After incubation for additional 4 h (5), samples are collected from the basolateral side (6). The collected samples are analysed in ELISA for the presence of IgG or albumin using anti-IgG or anti-albumin antibodies, respectively (7).

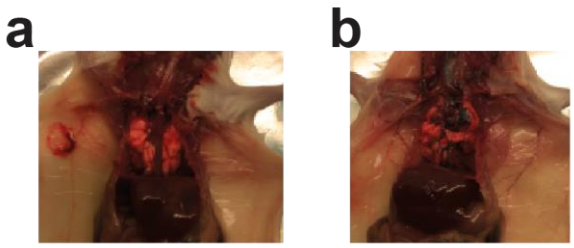

Figure S4. I.n. delivery of droplets ends up in the lungs of WT mice.

Mice were anesthetized and given either 1xPBS **(a)** or 1% Evans blue **(b)** i.n. followed by inhalation. After 20 minutes, the total blood was withdrawn and the mice were opened.

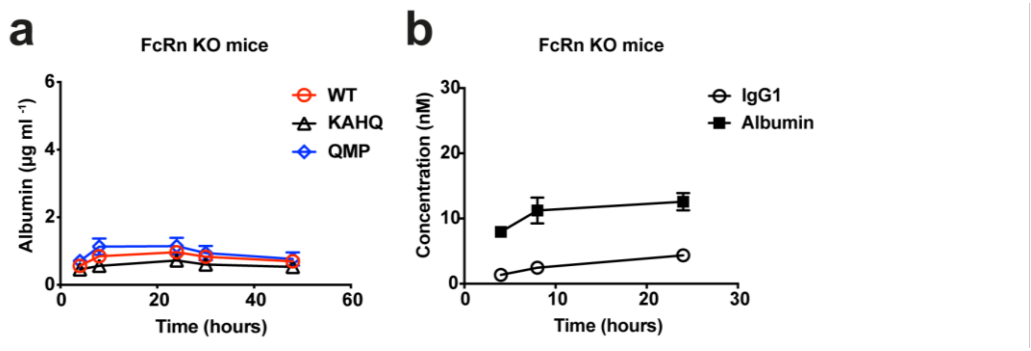

Figure S5. Pulmonary delivery of albumin and IgG1 to FcRn KO mice. Serum levels of albumin variants (µg ml^{-1}) **(a)** or IgG1 and WT albumin (nM) **(b)** given i.n. at a single dose, at 4, 8, 24, 30 and 48 hour time points **(a)** or 4, 8 and 24 hour time points **(b)** shown in connecting lines. Data are presented as mean ± s.e.m of six (**a**) or three (**b**) mice from one experiment.

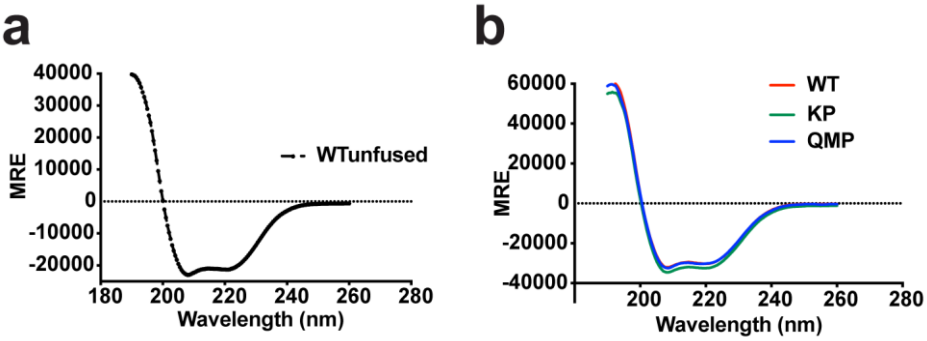

Figure S6. CD spectra of albumin variants.

Representative CD spectra of albumin (WT unfused) **(a)** and GST-fusions **(b)** obtained by CD measurements at pH 5.5. MRE; mean residual ellipticity. The secondary structural elements for each of the albumin variants are given in **Table S1**.

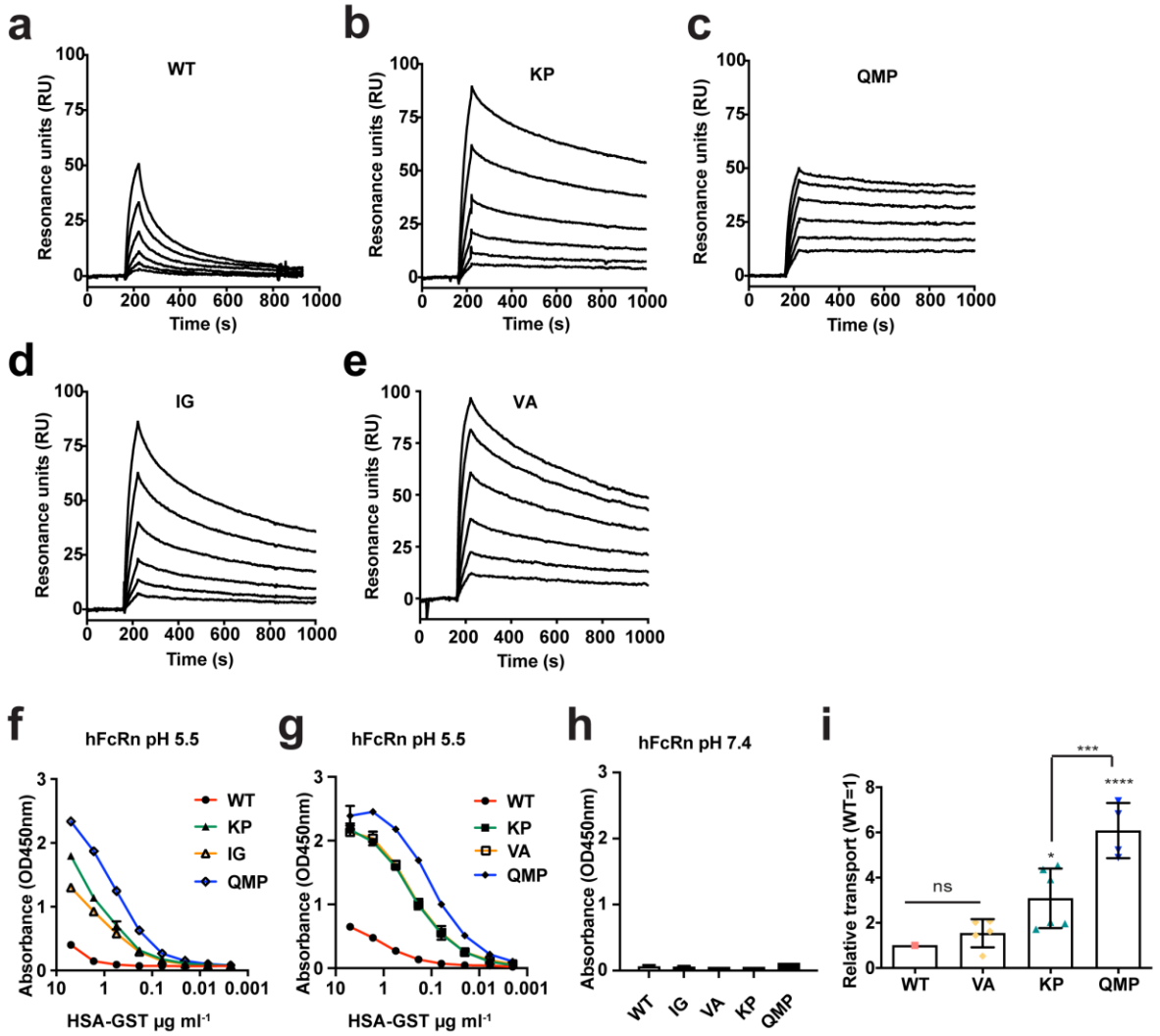

Figure S7. Human FcRn binding and transport properties of albumin-GST fusions.

(a-e) Representative SPR sensorgrams showing binding of titrated amounts of monomeric His-tagged human FcRn injected over immobilized albumin-GST variants at pH 5.5. The injections were performed at 25˚C and the flow rate was 50 µl min^{-1}. The kinetic rate constants were obtained using a simple first-order (1:1) bimolecular interaction model (Langmuir) supplied by the BIAevaluation 4.1 software. The kinetic values are summarized in **Table 1**. **(f-h)** Binding of His-tagged human FcRn (10 µg ml^{-1}) to titrated amounts (5-0,002 µg ml^{-1}) of albumin-GST variants at pH 5.5 (f-g) or pH 7.4 (h). Data sets are presented as mean ± S.D. **(i)** ELISA quantification of the amounts of A-B transport of GST-fused WT, VA, KP and QMP across polarized T84 monolayers after 4 hours. Relative transport of GST-

fused variants is calculated based on the pM/cm^2 values and WT is set to 1. Error bars indicate S.D. of up to six individual monolayers from one representative experiment out of three. *p <0.05, **p < 0.01, ***p < 0.001, ****p < 0.0001, ns: not significant, by one-way ANOVA test (Dunnett`s) (**i**). Graphs (f-i) are based on the same data sets shown in Figure 3f-h and 3i.

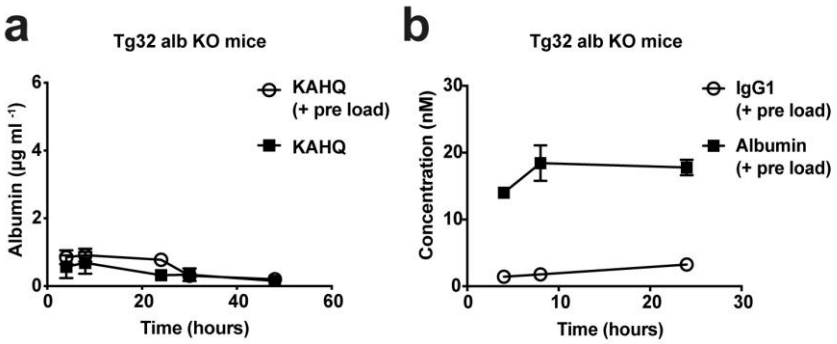

Figure S8. Pulmonary delivery of albumin and IgG1 to Tg32 alb KO mice and FcRn KO mice. (a) Levels of biotinylated KAHQ albumin (μg ml^{-1}) in blood samples from Tg32 alb KO mice with or without pre-loaded human albumin (3 mice/group) 4, 8, 24, 30 and 48 hours after i.n. delivery **(b)** Levels (nM) of IgG1 and biotinylated albumin in blood samples from Tg32 alb KO mice (6 mice/group) pre-loaded with human albumin or IgG 4, 8 and 24 hours after i.n. delivery.

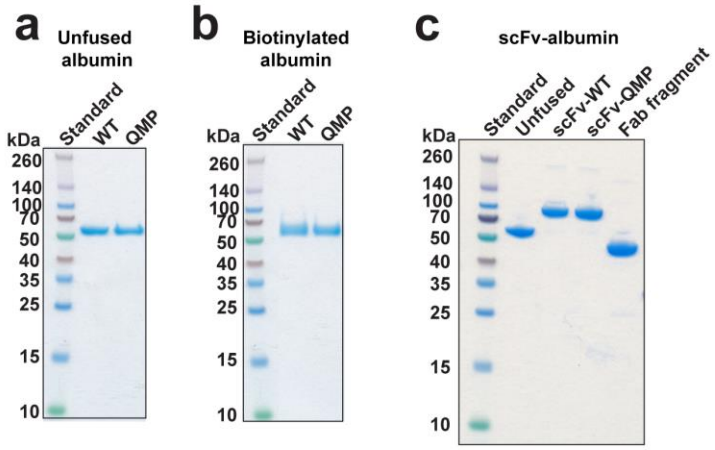

Figure S9. Non-reduced SDS page of different albumin formats.

Non-reducing SDS-PAGE gel showing migration of monomeric fractions of unfused albumin **(a)**, biotinylated albumin **(b)** or scFv-fused albumin and a Fab fragment **(c)**.

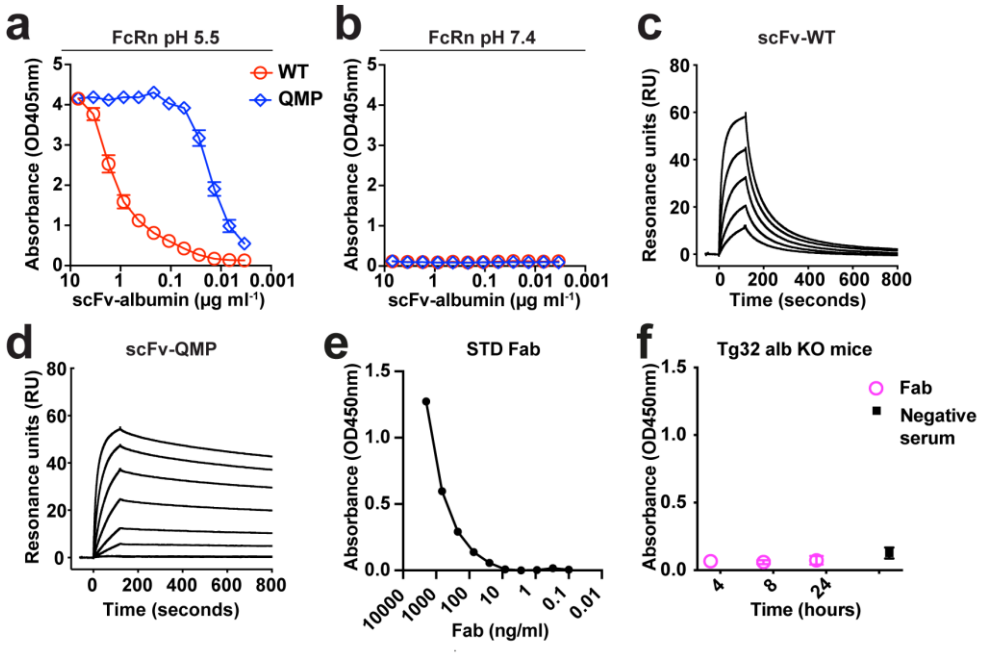

Figure S10. Binding of scFv-albumin fusions to human FcRn and pulmonary delivery of a Fab fragment to Tg32 alb KO mice. (**a-b**) Binding of His-tagged human FcRn (10 µg ml^{-1}) to titrated amounts (5-0,002 µg ml^{-1}) of scFv-albumin variants at pH 5.5 (**a**) or pH 7.4 (**b**). FcRn was captured on IgG1-MST/HN coated in ELISA wells and bound variants were detected using an ALP-conjugated anti-albumin antibody. All data are presented as mean ± S.D. (**c-d**) Representative SPR sensorgrams showing binding of titrated amounts (in the range of 1000-0.9 nM) of monomeric human FcRn injected over immobilized (~200 RU) scFv fused to WT albumin **(c)** or QMP **(d)** at pH 5.5. Injections were performed with a flow rate of 40 µl min^{-1} at 25°C. **(e)** Binding of titrated amounts (2000-0.1 ng ml^{-1}) of a Fab fragment to an ALP-conjugated antibody specific for human kappa light chains coated in ELISA plates followed by detection with HRP-conjugated Protein L. **(f)** Levels (µg ml^{-1}) of Fab fragment in blood given i.n. at a single dose to Tg32 alb KO mice pre-loaded with human albumin (3 mice per group) at 4, 8 and 24 hour time points shown in connecting lines. Serum from pre-loaded Tg32 alb KO mice was used as negative control (negative serum).

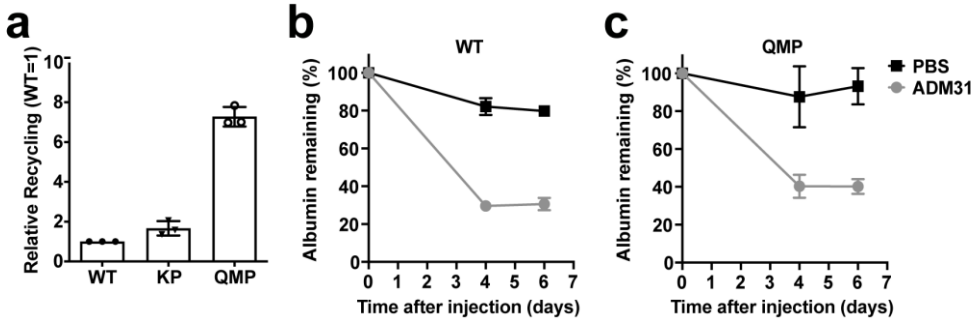

Figure S11. QMP is rescued from intracellular degradation in an FcRn-dependent manner. (**a**) HERA showing relative cellular recycling of WT human albumin, KP and QMP. Equal amounts of each variant (1000 nM) were incubated with HMEC1 cells for 4 hours, followed by extensive washing and another 4 hour incubation step before sample collection. The amounts of recycled albumin were quantified by ELISA and the obtained data are shown as mean ± s.d. of one representative experiment performed in triplicates. (**b-c**) Tg32 Alb KO mice received either 1x PBS (black line) or 1 mg ADM31 (monoclonal anti-human FcRn antibody) (grey line) on day 64 post injection of WT human albumin (**b**) or QMP (**c**). The serum levels are presented as percentage remaining in the circulation compared to that measured 64 days after injection of the albumin. The values represent the mean ± s.d. of two-three mice.

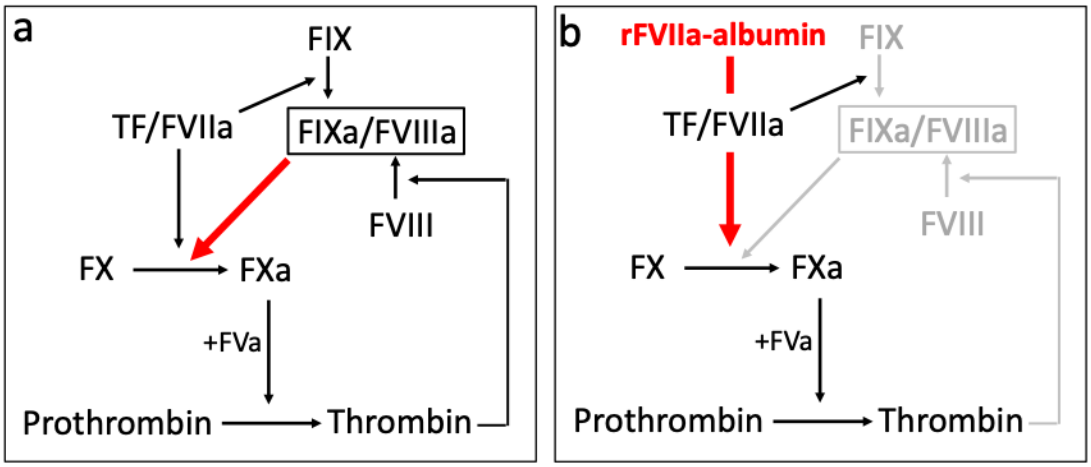

Figure S12. Schematic representation of physiological *versus* defective thrombin generation restored by rFVIIa-albumin in haemophilia.

(**a**) In normal conditions, activated coagulation factor VII (FVIIa), complexed with tissue factor (TF), cleaves and activates factor X (FX) and factor IX (FIX). Activated FX (FXa) binds activated factor V (FVa) and catalyzes the formation of small amounts of thrombin, which in turn activates factor VIII (FVIII). This acts as cofactor of activated FIX (FIXa), forming an essential complex that provides massive FX activation (red arrow), resulting in large-scale thrombin generation and finally in clot formation. (**b**) In haemophilia A or B, FVIII or FIX are missing, respectively. This virtually abolishes the essential feedback loop needed for massive FX activation and thrombin generation, leading to defective clot formation and bleeding phenotypes. Addition of rFVIIa-albumin by-passes the defective FVIII/FIX pathway and directly boost FX activation (red arrow), thereby restoring proper thrombin generation and clot formation.

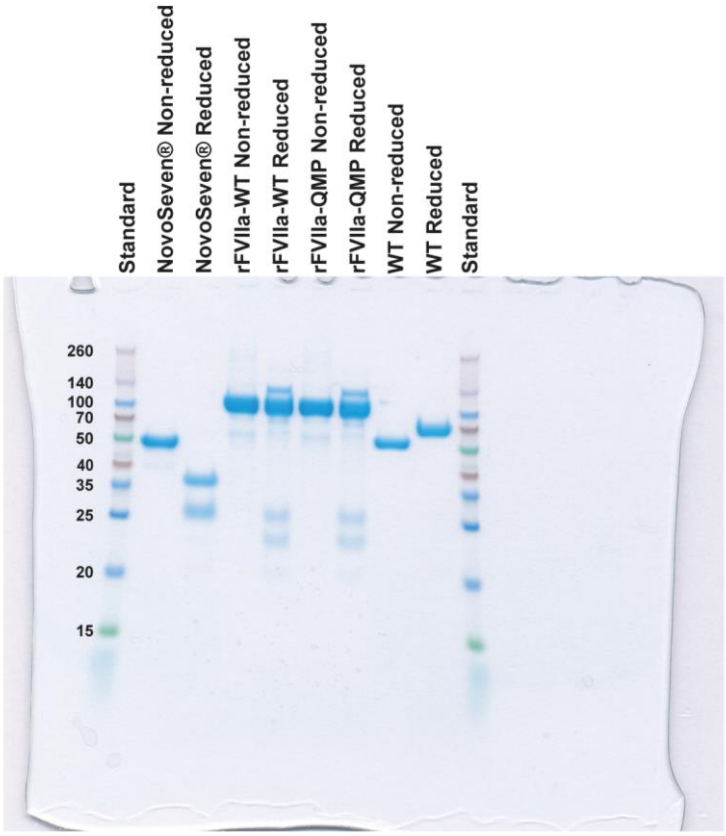

1523

1524 **Figure S13. SDS-PAGE analysis of rFVIIa-albumin fusions.**

1525 SDS-PAGE analysis of NovoSeven®, recombinant rFVIIa fused to wild-type or engineered

1526 (QMP) albumin and unfused WT albumin under non-reducing or reducing conditions.

1527

1528

1529

1530

1531

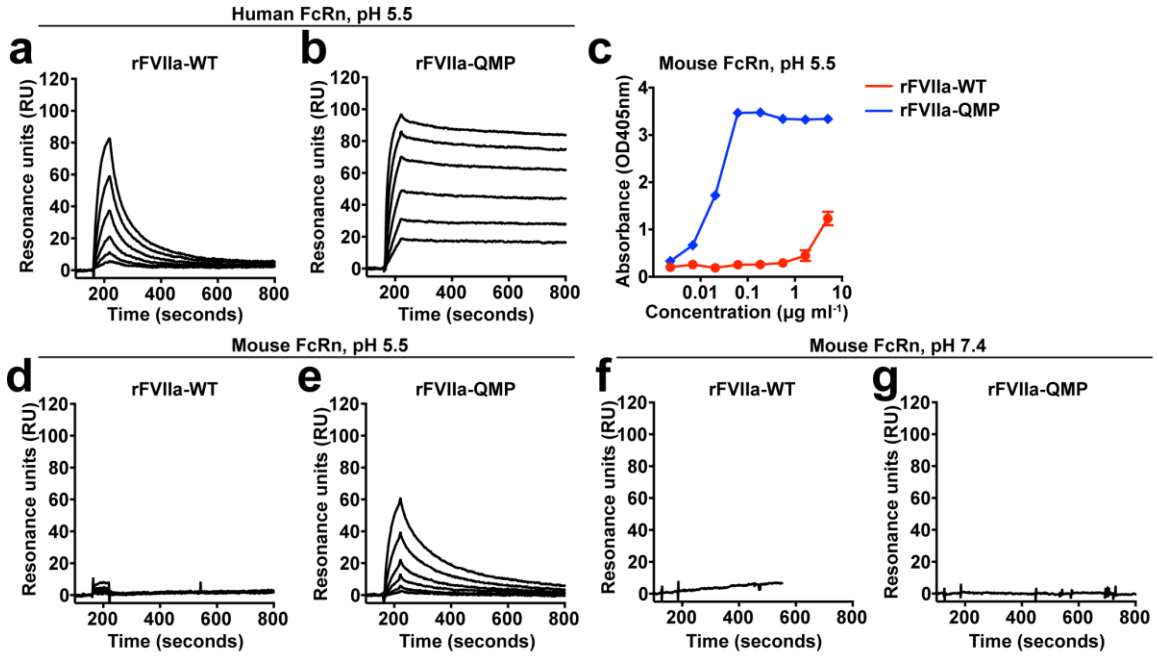

Figure S14. Binding of rFVIIa-albumin fusions to human and mouse FcRn. (**a, b**) SPR sensorgrams showing binding of titrated amounts (1000-31.5 nM) of monomeric human FcRn injected over immobilized (~500 RU) rFVIIa-WT **(a)** or rFVIIa-QMP **(b)** at pH 5.5. (**c**) ELISA showing binding of rFVIIa fused to WT albumin (red) or QMP (blue) to mouse FcRn at pH 5.5. The numbers represent the mean ± s.d. of duplicates from one representative experiment. (**d-e**) SPR sensorgrams showing binding of titrated amounts (1000-31.5 nM) of monomeric mouse FcRn injected over immobilized (~500 RU) rFVIIa-WT **(d)** or rFVIIa-QMP **(e)** at pH 5.5. (**f-g**) SPR sensorgrams showing binding of 1000 nM of monomeric mouse FcRn injected over immobilized (~500 RU) rFVIIa-WT **(f)** or rFVIIa-QMP **(g)** at pH 7.4. Injections were performed with a flow rate of 40 µl/min at 25°C.

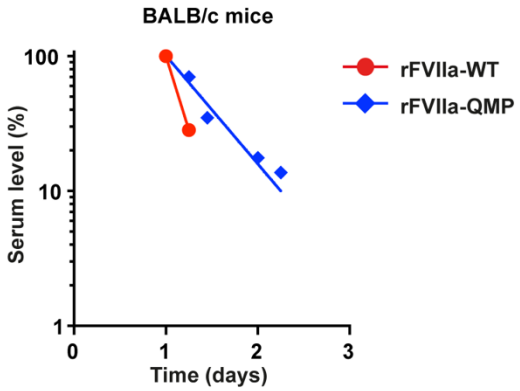

Figure S15. rFVIIa-QMP shows extended half-life in BALB/c mice. Elimination curves of rFVIIa-WT (red) and rFVIIa-QMP (blue) in BALB/c mice that received 2 mg kg^{-1} via intravenous injection. The serum levels are presented as percentage remaining in the circulation compared to that measured 1 day after injection. The values represent the mean ± s.d. of three mice.

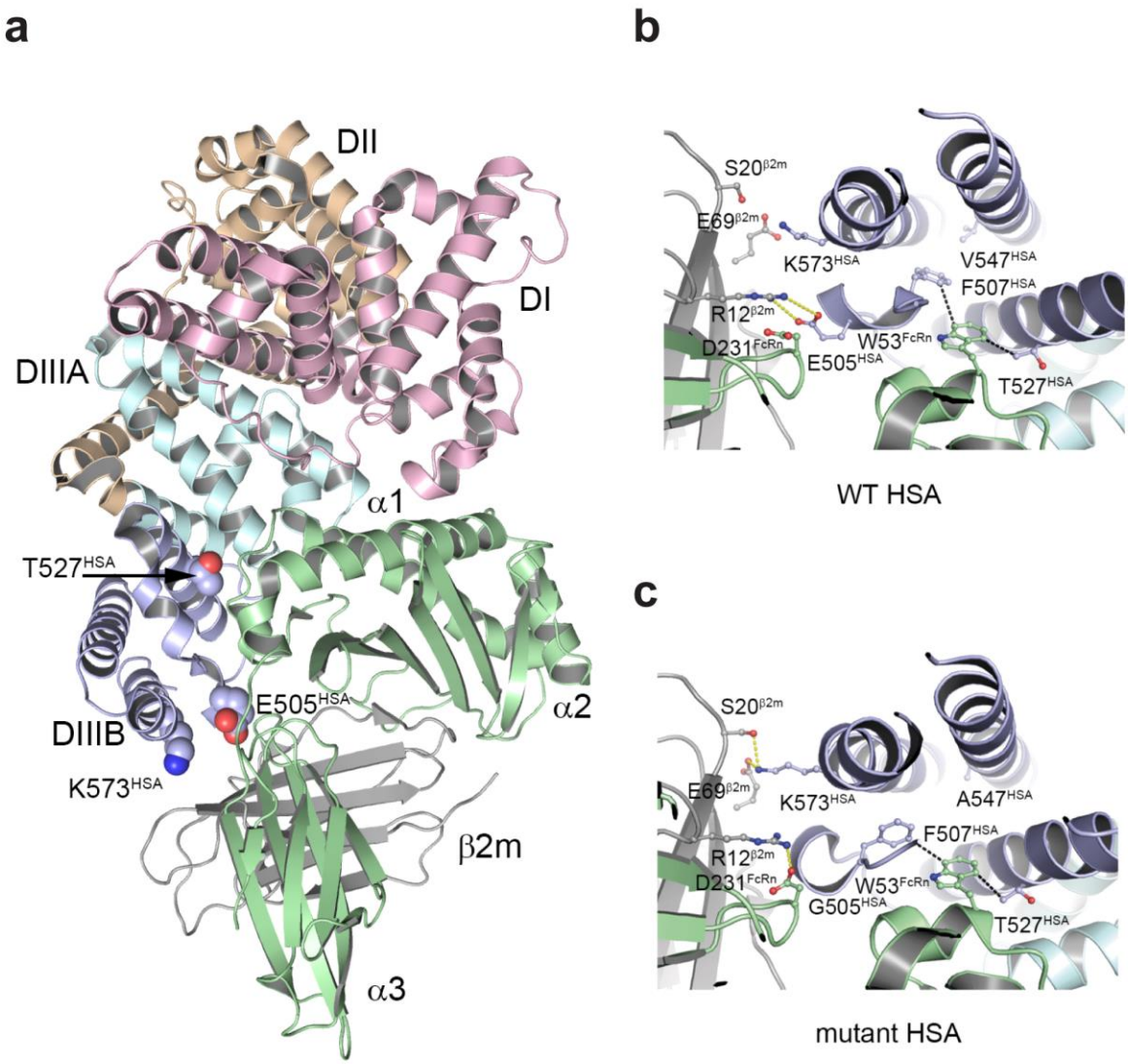

Figure S16. The co-crystal structure of binding of WT and mutant albumin to FcRn.

(a) Illustration of the co-crystal structure of human FcRn in complex with human serum albumin (HSA). HSA domain one, two and three (DI, DII and DIII) are highlighted in pink orange and cyan/blue, respectively, while the FcRn heavy chain (α1, α2 and α3) is highlighted in green and β2-microglobulin (β2m) in grey. Spheres in DIII show amino acid positions that have been mutated; E505, T527 and K573. A close-up of the interacting interface of **(b)** WT HSA and **(c)** HSA13 in complex with human FcRn with the amino acid positions involved and targeted in this study highlighted. T527 is in proximity to the hydrophobic W53 within an exposed loop of the α1-domain of the FcRn heavy chain, which

is crucial for albumin binding (*18-20*).(*18-20*). W53 is located between T527 and F507, and we hypothesized that replacement of T527 with the more hydrophobic methionine (TM) would cause tighter hydrophobic stacking and thus improve binding. In the co-crystal structure of HSA13, E505 is replaced with a glycine. However, we chose to mutate E505 to glutamine (EQ). E505 is located within a loop in close proximity to both the α1 and α2 domains of FcRn, and in the case of EQ, we speculated that removal of a negative charge would cause stronger contacts with the receptor, especially as FcRn-D231 also carries a negative charge. The figures were made using PyMOL with the crystal structure data of WT HSA-FcRn (*18*) and HSA13-FcRn (*20*).

Table S1. The content of α-helix and random coil determined by CD at pH 5.5		
Albumin variant	**α-helix (%)**	**Random coil (%)**
WT unfused	**64.9**	**21.7**
GST-fusions		
WT	**75.4**	**18.9**
KP	**75.6**	**18.1**
QMP	**75.1**	**18.7**

References

1. G. J. Christianson *et al.*, Monoclonal antibodies directed against human FcRn and their applications. *mAbs* **4**, 208-216 (2012).
2. K. M. Sand *et al.*, Interaction with both domain I and III of albumin is required for optimal pH-dependent binding to the neonatal Fc receptor (FcRn). *J Biol Chem* **289**, 34583-34594 (2014).
3. A. Grevys *et al.*, A human endothelial cell-based recycling assay for screening of FcRn targeted molecules. *Nature Communications* **9**, (2018).
4. M. Firan *et al.*, The MHC class I-related receptor, FcRn, plays an essential role in the maternofetal transfer of gamma-globulin in humans. *International immunology* **13**, 993-1002 (2001).
5. S. Popov *et al.*, The stoichiometry and affinity of the interaction of murine Fc fragments with the MHC class I-related receptor, FcRn. *Mol Immunol* **33**, 521-530 (1996).
6. a. Grevys *et al.*, Fc Engineering of Human IgG1 for Altered Binding to the Neonatal Fc Receptor Affects Fc Effector Functions. *The Journal of Immunology* **194**, 5497-5508 (2015).
7. J. T. Andersen, M. B. Daba, I. Sandlie, FcRn binding properties of an abnormal truncated analbuminemic albumin variant. *Clinical biochemistry* **43**, 367-372 (2010).
8. L. Norderhaug, T. Olafsen, T. E. Michaelsen, I. Sandlie, Versatile vectors for transient and stable expression of recombinant antibody molecules in mammalian cells. *J Immunol Methods* **204**, 77-87 (1997).

9. G. Berntzen *et al.*, Prolonged and increased expression of soluble Fc receptors, IgG and a TCR-Ig fusion protein by transiently transfected adherent 293E cells. *J Immunol Methods* **298**, 93-104 (2005).
10. L. S. Hoydahl *et al.*, Plasma Cells Are the Most Abundant Gluten Peptide MHC-expressing Cells in Inflamed Intestinal Tissues From Patients With Celiac Disease. *Gastroenterology* **156**, 1428-1439.e1410 (2019).
11. L. S. Høydahl *et al.*, Multivalent pIX phage display selects for distinct and improved antibody properties. *Scientific Reports* **6**, 39066 (2016).
12. P. Margaritis, Gene-based continuous expression of FVIIa for the treatment of hemophilia. *Frontiers in bioscience (Scholar edition)* **4**, 287-299 (2012).
13. A. Branchini *et al.*, The carboxyl-terminal region is NOT essential for secreted and functional levels of coagulation factor X. *Journal of thrombosis and haemostasis : JTH* **13**, 1468-1474 (2015).
14. T. Weimer *et al.*, Prolonged in-vivo half-life of factor VIIa by fusion to albumin. *Thrombosis and haemostasis* **99**, 659-667 (2008).
15. M. Ferrarese *et al.*, The carboxyl-terminal region of human coagulation factor X as a natural linker for fusion strategies. *Thrombosis research* **173**, 4-11 (2019).
16. G. Böhm, R. Muhr, R. Jaenicke, Quantitative analysis of protein far UV circular dichroism spectra by neural networks. *Protein engineering* **5**, 191-195 (1992).
17. A. W. Weflen *et al.*, Multivalent immune complexes divert FcRn to lysosomes by exclusion from recycling sorting tubules. *Mol Biol Cell* **24**, 2398-2405 (2013).
18. V. Oganesyan *et al.*, Structural insights into neonatal Fc receptor-based recycling mechanisms. *Journal of Biological Chemistry* **289**, 7812-7824 (2014).

19. K. M. K. Sand *et al.*, Dissection of the neonatal Fc receptor (FcRn)-albumin interface using mutagenesis and anti-FcRn albumin-blocking antibodies. *Journal of Biological Chemistry* **289**, (2014).

20. M. M. Schmidt *et al.*, Crystal Structure of an HSA / FcRn Complex Reveals Recycling by Competitive Mimicry of HSA Ligands at a pH-Dependent Hydrophobic Interface. *Structure* **21**, 1966-1978 (2013).